Multi-timescale neural adaptation underlying long-term musculoskeletal reorganization.

(Multi-timescale neural adaptation)

*Roland Philipp[1,2], Yuki Hara[3], Naohito Ohta[1,2], Naoki Uchida[1,2], Tomomichi Oya[1,4], Tetsuro Funato[2], and *Kazuhiko Seki[1]

[1]National Center of Neurology and Psychiatry, Department of Neurophysiology, 4-1-1 Ogawa-Higashi, Kodaira, Tokyo 1878502, Japan
[2]University of ElectroCommunications, Graduate School of Informatics and Engineering, Dept. of Mechanical and Intelligent Systems Engineering. W2-217, 1-5-1 Chofugaoka, Chofu, Tokyo, Japan
[3]National Center of Neurology and Psychiatry, Department of Orthopaedic Surgery, 4-1-1 Ogawa-Higashi, Kodaira, Tokyo 1878502, Japan
[4]Western Institute for Neuroscience, University of Western Ontario, London, N6A 3K7, Canada

*Corresponding authors:
Kazuhiko Seki and Roland Philipp
Email: seki@ncnp.go.jp and roland@ncnp.go.jp

Author Contributions: R.P. and K.S. designed all experiments and wrote the paper. R.P., Y.H., N.U., and N.O. performed the experiments and analyzed the data. R.P., Y.H., T.O., and K.S. performed the surgeries. T.F. provided conceptual advice and wrote the paper. All authors reviewed the results and approved the final version of the manuscript.

Conflict of Interest Statement: The authors declare no competing interests.

Number of pages: 74 (96, including supplementary text)
Number of figures: 10 (20, including supplementary figures)
Number of multimedia: 7
Number of words for abstract: 173
Number of words in introduction: 557
Number of words in discussion: 1436

ABSTRACT

The central nervous system (CNS) can effectively control body movements despite environmental changes. While much is known about adaptation to external environmental changes, less is known about responses to internal bodily changes. This study investigates how the CNS adapts to long-term alterations in the musculoskeletal system using a tendon transfer model in non-human primates. We surgically relocated finger flexor and extensor muscles to examine how the CNS adapts its strategy for finger movement control by measuring muscle activities during grasping tasks. Two months post-surgery, the monkeys demonstrated significant recovery of grasping function despite the initial disruption. Our findings suggest a two-phase CNS adaptation process: an initial phase enabling function with the transferred muscles, followed by a later phase abolishing this enabled function and restoring a control strategy that, while potentially less conflicted than the maladaptive state, resembled the original pattern, possibly representing a 'good enough' solution. These results highlight a multi-phase CNS adaptation process with distinct time constants in response to sudden bodily changes, offering potential insights into understanding and treating movement disorders.

SIGNIFICANCE STATEMENT

After major changes to the body's mechanics, the nervous system adapts motor control using strategies operating on multiple timescales. Our primate tendon transfer study shows that core muscle synergy groupings remain stable, reflecting modular control principles. However, the activation of these synergies changes substantially, with rapid initial shifts followed by slower adjustments over weeks. This process highlights the fundamental tension the CNS faces in balancing reliance on stable muscle synergies with the need for flexible control to manage new mechanics. Understanding this adaptive process offers insights into neural plasticity and informs potential rehabilitation strategies.

INTRODUCTION:

The central nervous system (CNS) adapts bodily functions in response to various challenges, including external changes like altered gravitational fields or altered sensory feedback (Sugita, 1996; Davidson and Wolpert, 2003; Luauté et al., 2009; Fleury et al., 2019). While such paradigms have provided models for motor adaptation to external perturbations, less is understood about adaptations to internal changes, such as growth (Power and Schlaggar, 2017), muscle fatigue (Green, 1997), postural sway (Zemková, 2022), disorientation from bodily rotations (Schärli et al., 2024), and structural alterations to the musculoskeletal system (Walker et al., 2004). Unlike external changes, which are often transient and predictable, internal changes, particularly structural alterations, require the CNS to remap motor control within the context of the body's altered biomechanics and sensory feedback. Although external tools can alter effective limb dynamics (Imamizu et al., 2000), our focus is on the CNS response to changes in the body's own physical structure. Understanding adaptation to such internal changes is crucial for understanding the pathophysiology of chronic conditions such as osteoarthritis or muscular dystrophy, where progressive musculoskeletal changes lead to significant motor dysfunction (Walker et al., 2004).

To manage the complexity of the motor system, the CNS may utilize modular building blocks such as muscle synergies, which coordinate groups of muscles into functional units (d'Avella et al., 2003; Bizzi and Cheung, 2013). Efficient motor control often relies on muscle synergies, reducing the degrees of freedom the CNS must control. However, skilled behavior, like dexterous hand movements, often relies on fractionation – the ability to selectively activate muscles independently. For instance, precise finger movements like typing or playing a musical instrument require a high degree of fractionation. This creates a tension: how does the CNS balance the stability and efficiency of modular synergistic control with the flexibility needed when the musculoskeletal system undergoes change? Does adaptation rely on modulating existing synergies or developing more fractionated control?

Here, we use a tendon transfer (TT) surgery model to explore how animals adjust limb control following long-term musculoskeletal changes. The TT model offers a unique perspective on CNS plasticity in response to altered internal physical environments (Sperry, 1940), contrasting with CNS lesion models where the injury itself complicates assessing adaptive capabilities. Tendon transfer provides a unique model to study CNS adaptation to altered musculoskeletal mechanics

because it creates a relatively well-defined and localized change, allowing researchers to isolate the effects of altered biomechanics from other confounding factors. Tendon transfer is used in various species, with studies suggesting different adaptive capacities, ranging from limited adaptation in adult rodents (Sperry, 1940; Sperry, 1942; Slawinska and Kasicki, 2002; Bowlus et al., 2003) to more substantial adjustments in cats (Yumiya et al., 1979; Loeb, 1999) and primates, including humans (Lee and Seung, 1999; Wester et al., 2018; Gaetz et al., 2023). Adaptability to TT appears enhanced in primates and humans. However, the organization and temporal progression of CNS adaptations post-TT remain unclear. This study aimed to identify long-term adaptive mechanisms of the primate CNS to musculoskeletal changes. We surgically altered the musculoskeletal system via crossed tendon transfer of finger extensor and flexor muscle tendons. We focused on determining how these modifications impact CNS regulation of limb muscle activity during recovery, with finger-grasping task control serving as the primary metric for assessing functional adaptation. Through this analysis, we sought to better understand long-term CNS adaptations to substantial musculoskeletal changes.

RESULTS

In this study, we developed a novel crossed tendon transfer animal model. This involved surgically swapping the tendons of two antagonistic finger muscles in a macaque monkeys' forearm (Fig. 1). The effectiveness and consistency of the surgery was confirmed by measuring: (i) the distance traveled by muscle fibers and their intramuscular tendons in the transferred muscle (Fig. 2B, C); and (ii) the amount of fingertip displacement (Fig. 2D, E). Both measurements were induced by percutaneous electrical stimulation over the transferred muscles (Fig. 2A). For a detailed description of the results of these measurements see the Methods section. Here, we will primarily discuss the adaptations observed by electromyography (EMG) post-tendon transfer (TT), as well as behavioral recovery in the monkey. The two monkeys were assigned slightly different tasks, allowing us to examine controlled grasping in Monkey A and a more natural grasp in Monkey B (refer to the Methods section, and Figs. 2, 3 and S1 for further details). Once the monkeys had mastered their respective tasks, we recorded control sessions and then performed the crossed tendon transfer. Post-surgery, and once the monkeys had fully recovered and were able to perform the task independently (~3–4 weeks), EMG recordings and behavior were examined.

Despite the now reversed roles of the transferred muscles, the monkeys were able to recover their grasping performance within two months (Fig. 4). Functional recovery was primarily assessed based on the return of key behavioral metrics, such as object/food contact time (Fig. 4), to pre-surgical baseline levels, as well as the animal's consistent ability to perform the task independently without assistance (see Methods and Supplementary Video legends). However, none of the parameters measured returned promptly to pre-TT levels. For example, contact time with the object (Monkey A, Fig. 4A) or food (Monkey B, Fig. 4C) were much longer immediately after TT than in the first 6 (or 5) sessions post-TT (197.7 ± 92.2 vs. 660.6 ± 221 ms; $p = 0.014$, and 169.7 ± 14 vs. 316.3 ± 31.9 ms; $p = 0.016$, respectively. Two-sample *t*-test; mean ± SD; filled squares in Fig. 4). It took around 10 days for both monkeys to recover back to pre-TT levels ($p > 0.05$, two-sample *t*-test) and fully stabilize (after 20 and 32 days, respectively). All measured indices eventually returned to pre-TT levels by the end of the experiment.

155 ***Transferred muscles exhibited antagonistic EMG activity post-TT***

156 Initially, we investigated whether EMG activity exhibited any changes post-TT.
157 Given that we interchanged the tendons of an antagonistic muscle pair,
158 functionally rendering the FDS an extensor and the EDC a flexor (as confirmed
159 mechanically, Fig. 2), a biomechanically sound adaptation would be to use the
160 former finger extensor (EDC) for finger flexion, and the former finger flexor (FDS)
161 for finger extension during a grasping task. Our focus was to determine if these
162 expected changes did indeed occur by EMG of both the transferred and non-
163 transferred muscles.

164 Figure 5 shows a comparison of EMG activity profiles for the two transferred
165 muscles, EDC and FDS, in Monkey A (Fig. 5C–F). Prior to surgery, the control
166 showed distinct and contrasting EMG profiles in both muscles. For instance, peak
167 activity in EDC (▼) occurred long after completion of the grasping action
168 (indicated by vertical dashed lines at 0% task range) at 15% task time (Fig. 5C),
169 coinciding with the animal pre-shaping its hand to prepare for the subsequent
170 grasp. Whereas peak activity in FDS (▽) was observed immediately after
171 completion of the grasping action (0.49%; Fig. 5E). The question we posed was

172 whether the post-surgery activity of EDC resembled its original profile (without
173 adaptation to surgery) or the activity of FDS (the anticipated profile following
174 surgical adaptation), and vice versa. Our findings suggested that EMG activity
175 patterns largely shifted in a manner consistent with the new mechanical function
176 imposed by the transfer. Early after TT, peak activity of EDC occurred at -0.58%
177 task time (Fig. 5D; days 29 [red line] and 64 [orange]), which aligns with peak
178 activity of FDS prior to TT (Fig. 5E; black line). Also, for FDS, peak activity
179 occurred at 11% task time (Fig. 5F; ▼), which aligned with peak activity of EDC
180 (Fig. 5C).

181 This was corroborated by the results in Monkey B (Fig. S2). Although the EMG
182 patterns of both muscles varied significantly as the two monkeys performed
183 different types of grasping actions, we found that the EMG of EDC peaked at -
184 6.12% before (Fig. S2A; ▼) and 0.35% and 1.05% after TT (Fig. S2B; ▽, days
185 22 and 36, respectively), closely matching the timing for FDS control data (Fig.
186 S2C). Note that the corresponding analysis using FDS could not be performed in
187 Monkey B, since the EMG signal of FDS was lost early after TT (see Methods for
188 details).

189 We were able to extend our recordings to 122- and 64-days post-TT for monkeys
190 A and B, respectively. This allowed us to examine whether the adaptations
191 observed in the early period were consistent throughout the experimental period.
192 These additional days (Fig. 5D, F; 69 [cyan], 79 [blue], and 99 [black] post-TT;
193 see Fig. S3 for recordings from all days) showed that the EMG activity profiles for
194 both muscles unexpectedly returned to their pre-surgery state. For example, as
195 already described, the EMG signal of EDC at days 29 and 64 shared the
196 characteristics of FDS, but by the following day (only 5 days later, day 69 [light
197 blue] post-TT) already exhibited pre-TT characteristics of EDC, continuing as
198 such until the end of the recording period (day 79 [blue] and 99 [black]). This was
199 confirmed for the EDC muscle of Monkey B (Fig. S2A, B; Fig. S3U-AO for
200 recordings from all days).

201 Figure 5G illustrates cross-correlation coefficients between the EDC EMG profile
202 post-TT (EDC-post) and the original EDC control data (EDC-pre) in Monkey A.
203 Figure 5I shows coefficients for EDC-post and FDS-pre correlations in the same
204 monkey. The coefficient corresponding to the original profile decreased to
205 between -0.3 and 0.2 over approximately 65 days (Fig. 5G). In contrast, the
206 coefficient corresponding to the expected EMG profile exhibited an inverse

207 pattern, with low coefficients pre-TT and a high coefficient (of 0.9) post-TT (Fig.
208 5I). Cross-correlation analysis for FDS (Fig. 5H–J) revealed a similar pattern.
209 Cross-correlation coefficients for FDS-pre- vs. FDS-post-analysis declined from
210 1 to negative values, only to rebound to their original values within a month (day
211 79; Fig. 5H). This outcome aligns with our previous observations (Fig. 5D, F), and
212 were corroborated by the results from Monkey B (Fig. S2). Here, cross-correlation
213 coefficients dropped from +0.95 to +0.1 for EDC-pre vs. EDC-post comparison,
214 and increased from -0.5 to 0.9 for the FDS-pre- vs. EDC-post comparison (Fig.
215 S2D, E). After 42 days post-TT, cross-correlation coefficients started to gradually
216 increase or decrease to +0.9 and -0.7, respectively. This indicates that the
217 anticipated initial changes in EMG activity profiles are not permanent. Instead,
218 they revert to their original patterns two months post-TT.

219 In summary, both monkeys exhibited a distinct two-phase adaptation following
220 TT. We define the 'early phase' as the period from initial post-surgical recovery
221 up to the reversal of the swapped activation patterns (approximately days 20/29
222 to ~65 post-TT, see Fig. 7), characterized by the transferred muscles/synergies
223 adopting antagonistic temporal profiles. The 'late phase' encompasses the period

following this switch-back (after ~day 66 post-TT), where original activation timings were largely restored.

Non-transferred muscles exhibited characteristic changes in EMG activity post-TT

Interestingly, changes in EMG pattern were not isolated to the transferred muscles. When the analysis was repeated on non-transferred muscles in both monkeys (Figs. S3–5), we also found comparable changes in some muscles. This quantitative analysis is described in the next section; here, we briefly describe activity characteristics. In Monkey A, similar changes as in the EDC (Fig. 5C, D) were also found in extensor digitorum-2,3 (ED23), extensor carpi ulnaris (ECU), and extensor carpi radialis (ECR) (Fig. S4B–D and L–N), i.e., an initial shift of activity towards pre-surgery FDS that was followed by a later reversion to the original pattern. The non-transferred flexor carpi ulnaris (FCU) (Fig. S4G, Q) exhibited changes that mimicked those observed in FDS (Fig. 5E, F). We found that the non-transferred muscles in Monkey B (Fig. S4U-AO) also exhibited the changes observed in the transferred muscles. For example, ED23, ED45, ECU,

241 and flexor digitorum profundus (FDP) (e.g., ED23; Fig. S4AH) exhibited similar
242 changes as in EDC (Fig. S4AG), initially adopting flexor properties and later
243 reverting to their original pattern.

244 In addition, some muscles also exhibited a patten that was incompatible with the
245 transferred muscles. For example, before TT, PL, and flexor carpi radialis (FCR)
246 exhibited peak activity at event alignment in monkey A (e.g., PL at object
247 release; Fig. S4H, I), which again increased gradually over time towards the end
248 of the shown task range. After TT, however, the amplitude of both peaks initially
249 decreased drastically, followed by a consistent increase in the amplitude of the
250 later peak. There was no two-step change observed in the transferred muscles
251 in any of the subsequent recording days (Fig. S4R, S).

252

253 ***Muscle synergies exhibited antagonistic properties post-TT***

254 Alternation of EMG activity in non-transferred muscle suggests an interesting
255 possibility: TT might alter the control strategy of coordinated muscle activity for
256 hand movement by modifying the transferred muscles and their agonists as a
257 cohesive unit (i.e., muscle synergy). To test this, we conducted a similar analysis

258 on temporal activation coefficients of muscle synergies. We computed synergy
259 weights (Fig. 6A–D and S7A-D for Monkey A; and Fig. S6A-D and S7E-H for
260 Monkey B) and temporal activation coefficients (Fig. 6E–H for Monkey A; and Fig.
261 S6F–I for Monkey B) from EMGs using non-negative matrix factorization (NMF)
262 (Lee and Seung, 1999). We extracted four muscle synergies that accounted for
263 more than 80% (Cheung et al., 2012) of the 'variance accounted for' (VAF) (Figs.
264 6E and S6E, 85% for both monkeys; the results of the original and shuffled data
265 sets are shown). Among these synergies, one was a finger flexor synergy and
266 another was a finger extensor synergy, identified before the crossed tendon
267 transfer in each monkey (Fig. 6A, B and S7A, B). These were referred to as
268 synergy A and synergy B, respectively.

269 We examined if the composition and activation coefficient of each synergy
270 changed, corresponding to the changes observed in the transferred and non-
271 transferred muscles. First, we analyzed changes in the composition of these
272 synergies. The cosine distance for the same synergy pairs (e.g., synergy A of
273 pre-TT and synergy A of post-TT in all recording days (Fig.S7A, E; monkey A and
274 B, respectively) was low (mean [± SD]: 0.03 [± 0.03] in Monkey A and 0.09 [±
275 0.11] in Monkey B) and different pairs (e.g., synergy A of pre-TT and synergy B

276 of post-TT) was high (mean [± SD]: 0.67 [± 0.08] in Monkey A and 0.61 [± 0.14]
277 in Monkey B). There was a one-to-one correspondence between synergy pairs
278 ($p < 0.0001$, two-way analysis of variance [ANOVA] due to synergy factor; $p <$
279 0.01, Bonferroni post-hoc test between synergy of the same pair and different
280 pair). This was demonstrated in both monkeys (S7A-D and E-H for monkey A and
281 B, respectively). These results indicate that the composition of these four
282 synergies and the contribution of each muscle do not change drastically before
283 and after TT surgery.

284 Figure 6F–I presents a comparison of the activation coefficients for all four muscle
285 synergies, before and after the TT procedure (for Monkey B, refer to Fig. S6F–I;
286 Fig. S8 for all experimental days). Prior to TT, the activation coefficients for the
287 flexor synergy (synergy A) reached a peak at +0.97% (Fig. 6F). Post-TT, these
288 coefficients shifted towards later times shortly after surgery (+10.7%), but
289 eventually returned to their original timing. Meanwhile, the extensor synergy
290 (synergy B) peaked at 12.62% pre-TT and moved to -0.97% shortly after surgery.
291 Like the flexor synergy, the extensor synergy also reverted to its original timing in
292 subsequent sessions (Fig. 6G). These characteristics corresponded well to the

293 ones found in the transferred muscles (Fig. 5), supporting our hypothesis that the
294 transferred muscle and its agonist changes as a cohesive unit.

295 Figure 6H shows the temporal changes for synergy C, a wrist flexor synergy (Fig.
296 6C and S7C). While two peaks were observed prior to surgery (+1.46% and
297 +15%), the early post-surgery sessions did not exhibit any significant peaks.
298 However, later sessions displayed a single peak at +14.6% task time, with an
299 increasing magnitude as a function of recovery days. These characteristic
300 changes corresponded well to a patten that was incompatible to the transferred
301 muscles found in FCR and PL, as described above. Indeed, both muscles
302 showed highest synergy weights for this synergy (Fig. 6C and S7C). Synergy D
303 was a wrist extensor synergy (Fig. 6D and S7D), and underwent a single notable
304 change on day 29, but quickly reverted to its original pattern (Fig. 6H). These
305 pattens of changes in synergy 3 and 4, both contributed minimally to the EMG of
306 transferred muscles. This suggests that some non-transferred muscles change
307 their EMG activity following the mode, which is independent to the one observed
308 in the transferred muscle and may reinforce the functional adaptation made by
309 the transferred muscle and its synergists.

310 Several of these results were also confirmed in Monkey B. Activation coefficients
311 of extensor synergy B peaked at -8.75% before TT, increasing to +3.5% after TT
312 (Fig. S6G). This peak activity persisted until the last day (day 69 post-TT), when
313 it shifted back to an earlier time than -10% of the task range. This pattern
314 corresponds well to that found in the transferred muscles (EDC; Fig. S2).

315 Again, the characteristics of these changes in activation coefficients of muscle
316 synergies were also quantitatively confirmed by cross-correlation analysis of all
317 four muscle synergies. The coefficients were plotted over the course of
318 experimental days in relation to tendon surgery (Fig. 7). In this analysis, the
319 activation coefficient of each synergy was cross-correlated with either the one
320 from synergy A (finger flexor synergy; Fig. 7C, D, G, H) or synergy B (extensor
321 synergy; Fig. 7A, B, E, F) before TT. As previously demonstrated for the FDS and
322 EDC muscles, the temporal activation coefficients of muscle synergies A and B
323 (flexor and extensor) displayed a distinct pattern. After cross-correlation with their
324 own control data, both the flexor and extensor synergies showed coefficients of
325 1 prior to surgery. These became negative for 66 days post-surgery before
326 reverting close to their original values (Fig. 7B, C). However, after cross-
327 correlation with control data of the antagonistic muscle synergy (i.e., extensor for

flexor synergy and vice versa, Fig.4A, D), the pattern was reversed. Coefficients started with negative values prior to TT and shifted to positive coefficients near 1 shortly after surgery. Around 66 days later, the correlation coefficients returned to negative values. In short, these results mirror our findings between the transferred muscles (Fig. 5G, H). For synergies C and D, the changes in cross-correlation coefficients over time were markedly different. For synergy C, coefficients begin to steadily increase when cross-correlated with control data of the extensor synergy (synergy B, Fig.4E), and decreased with the flexor synergy (synergy A, Fig.4G). This suggests an increasing contribution to finger extension. In contrast, synergy D does not exhibit any specific pattern following TT. We also found a differential pattern of adaptation between transferred and non-transferred muscles in Monkey B (Fig. S9F-H).

Overall, we observed early and late changes between two synergy pairs (synergy A and B) in both monkeys, performing controlled and natural grasping. Another characteristic change that reinforced finger extension in other synergies was also observed (i.e., synergy C in Monkey A).

345 ***Rationale for the early reverse and late switch-back changes***

346 So far, our results suggest a two-step adaptation following TT: an early and a late
347 phase. In the initial (early adaptation) phase, the temporal activation patterns of
348 the transferred muscles and their host synergies largely shifted consistent with
349 their new mechanical roles (Figs. 2-4). However, the later phase restored pre-TT
350 EMG profiles and muscle synergies.

351 This two-step adaptation raises a key question: why? The early changes (where
352 extensor muscles exhibited flexor properties and vice versa) seem reasonable
353 and might be unique to CNS adaptation of non-human primates to TT. However,
354 the later reversal seems puzzling. The monkeys were already performing the task
355 relatively well (e.g., Fig. 4). Why did the early adaptation need to switch back to
356 the original pattern?

357 Here, we hypothesize that the TT forced the monkeys to explore new control
358 strategies of both transferred and non-transferred muscles (early adaptation),
359 and the reversing activity was a consequence of the monkey's exploitation of the
360 previous strategy. This hypothesis assumes that the early adaptation was a
361 "maladaptation" resulting from a now conflicting mechanical outcome of the

agonistic muscles (i.e., transferred vs. non-transferred muscles). For example, in monkey A, the finger extensor synergy (synergy B) is composed of EDC, ED23, and ED45, and their combination remained unchanged after TT and recovery (Fig. 6A–D and S7A–D). However, the transferred EDC became an anatomical finger flexor, while ED23 and ED45 continued to be anatomical extensors. This led to paradoxical activation of synergistic muscles with the finger extension synergy having similar activity to the finger flexion synergy. Therefore, after early adaptation, monkeys needed to establish a novel strategy to control the altered musculoskeletal systems. Early maladaptation must have triggered this exploring process.

This hypothesis appears to be supported by two additional observations. First, we found unusual behavioral characteristics during target reaching and grasping after TT (Supplementary Videos S2, S3, and S6). We compared the kinematic performance of grasping during early adaptation, late adaptation, and pre-TT periods. Following TT, monkeys exhibited clear functional impairments during the early adaptation phase before eventually recovering proficiency (Figs. 4). Behavioral observations revealed specific difficulties impacting fundamental reach control: Monkey A often required external assistance or support from its

contralateral limb to lift its forearm and displayed prolonged 'explorative' finger movements before achieving a grasp (Supplementary Video S2); Monkey B frequently overshot the target and collided with parts of the apparatus (Supplementary Video S6). Quantitative analysis confirmed these periods of impaired motor control, showing significantly increased durations for key behavioral events, such as contact times (Figs. 4A, C), and increased time spent in non-task-related workspace areas (Figs. 4B, D). These specific maladaptive reaching behaviors gradually diminished over several weeks, largely resolving by approximately day 70-75 post-surgery in Monkey A and day 60-65 in Monkey B (Figs. 4; Supplementary video S4 and S7). This early post-surgical behavior is considered maladaptive as it reflects substantially reduced movement efficiency and control precision (e.g., needing assistance, longer task/contact times, overshooting, ineffective finger movements), likely stemming from the profound changes in sensorimotor feedback and consequently inaccurate internal models resulting from the surgically altered musculoskeletal system. These observations were further supported by measuring the time spent for this maladaptive behavioral component in both monkeys (Figs. 4B, D). Monkey A exhibited malcoordinated reaching from day 29 (1978 ± 715 ms) to 73 (93.4 ± 3.7 ms) (see

398 Methods for additional details). The duration decreased progressively over time.
399 Monkey B showed malcoordinated reaching from day 20 (103.4 ms) to 62 (107.6
400 ms). The duration peaked at days 38–46 (167 ±1.4 ms) and then declined.
401 Notably, the periods dominated by malcoordinated movements coincided with the
402 observed maladaptive swapping of synergy A and B activity, occurring between
403 the early and late adaptation phases. This precise temporal coincidence between
404 the flawed synergy activation strategy and the behavioral impairments provides
405 strong support for the hypothesis that the maladaptive neural control directly
406 contributed to the observed impairments in reach control.

407 Second, we found that the net activity of muscles representing certain muscle
408 synergies (aggregated average EMG; aaEMG) were unstable during the period
409 between early (reversal) and late (switch-back) adaptation in their temporal
410 activation patterns (Fig. 5). In Monkey A (Fig. 8; see Fig. S10 and Extended result
411 in SI Appendix for Monkey B), muscles of the finger flexor synergy (synergy A,
412 Fig. 8A) tended to show a decrease in aaEMG post-TT, maintaining this lower
413 activity level throughout the experiment (p = 0.0004 at day 79, two-sample t-test,
414 Bonferroni-corrected; α = 0.01; panel E). Because the monkeys performed
415 successful grasping after TT, this suggests that finger flexion is performed by

muscles other than synergy A. The finger extensor synergy (synergy B, Fig. 8B) demonstrated a steady increase in aaEMG post-TT until day 64 ($p < 0.0001$, two-sample *t*-test, Bonferroni-corrected; $\alpha = 0.01$, panel F), when the activity abruptly reverted to near its pre-TT level. Increased activity of synergy B suggests a maladaptive attempt by the monkey to achieve finger flexion. This strategy involved enhancing activity of synergy B (which includes the EDC muscle, an atomical flexor) after TT. However, as previously established, this approach cannot effectively promote finger flexion, leading to eventual abandonment by the monkey. This 'arms race' dynamic, evidenced by the escalating aaEMG, directly reflects the mechanical conflict hypothesized to arise from activating the EDC (now acting as a flexor due to the transfer) within the extensor synergy, further supporting the idea that this maladaptive state drove the search for alternative strategies. While directly proving the causal chain is difficult, this hypothesis provides a plausible framework linking the observed mechanical conflicts, behavioral deficits, and multi-stage neural adaptation.

433 ***Recruitment of novel, compensatory movements aiding finger extension***

434 Muscles of synergy C (wrist flexion synergy) initially showed significantly
435 decreased aaEMG post-TT (days 69 and 79: $p < 0.0001$ and $p = 0.001$,
436 respectively; two-sample *t*-test, Bonferroni-corrected; $\alpha = 0.01$, panel G) but
437 showed a gradual increase starting from day 64. This is consistent with the cross-
438 correlation analysis (Fig. 4E), where cross-correlation coefficients between
439 synergy C (wrist flexor) and synergy B (finger extensor) initially dropped post-TT
440 but then first rapidly and then steadily increased over time. Increased reliance on
441 synergy C following TT suggests a compensatory strategy to overcome the
442 difficulty in finger extension, crucial for grasping. This is despite the recruitment
443 of the finger extensor and wrist flexor synergies, which seemed inadequate to
444 achieve effective flexion. The interactions between the cumulative proximal-to-
445 distal joint angles and musculo-tendon length can be complex. In our experiments,
446 as in human patients who receive tendon transfers (Zajac, 1992), those
447 interactions can affect the ranges of finger flexion-extension that can be achieved
448 for a given wrist angle (i.e., *passive and active tenodesis*). Briefly,
449 biomechanically, wrist flexion can enable finger extension (i.e., a dynamic
450 tenodesis where extensor tendons of the fingers cross both the wrist and

interphalangeal joints): Finger extension can cancel out the increase in total musculo-tendon length produced by wrist flexion. This compensatory interaction across joints allows for some degree of functional hand use, even in the absence of active finger movement (Cash and Jones, 2011) (see the Discussion for a complete description).

Further kinematic analysis of Monkey B (Fig. 9; no analysis on Monkey A due to low-resolution video images) indicated that this monkey indeed exhibited a similar active tenodesis as human patients. The angle at the metacarpophalangeal (MCP) joint, responsible for finger extension, steadily increased (Fig. 9A) after surgery, indicating finger extension. Concurrently, the wrist joint angle decreased (Fig. 9B), indicating wrist flexion. This coordinated movement suggests a compensatory strategy to achieve finger extension during grasping. Statistical analysis confirmed that MCP and wrist joint angles differed significantly between pre- and post-TT ($p < 0.0001$, ANOVA; $\alpha = 0.01$). Therefore, we suggest that deteriorated finger extension after TT was assisted by a compensatory wrist flexion synergy.

468 ***What triggered the late adaptation?***

469 Assuming that TT caused maladaptation and forced the monkeys to explore new
470 control strategies of both transferred and non-transferred muscles, what triggered
471 the late adaptation and why did the grasping performance increase after this
472 adaptation? To address this question, we summarized our experimental results
473 in a simple model (Fig. 10) consisting of multiple adaptation processes to TT with
474 different time constants: a slow dynamics adaptation (developing over
475 weeks/months, e.g., compensatory changes) and a fast dynamics adaptation (i.e.,
476 processes occurring rapidly over days, such as the switch-back event). In this
477 model, tendon cross-transfer surgery (black arrow) evoked changes in
478 coordination of finger muscle activity (i.e., swapping temporal activity of flexor
479 and extensor synergies; left blue arrow). These changes were sufficient to reach
480 a threshold (blue dotted line) and trigger (arrow 1) adaptation with slow dynamics
481 (A and B). This slow process may have different time constants. For example,
482 synergy B (Monkey A), which comprises EDC and ED23/ED45, consistently
483 elevated its activity to achieve successful flexion after TT (red line “A”). This ‘arms
484 race’ is instigated by conflicting activation of the ‘new flexor’ (EDC) and its
485 previous agonists (ED23/45), which still mechanically function as finger extensors.

In contrast, synergy A can reduce its activity as does synergy D (containing FDP), and accomplish the necessary finger flexion by simply adjusting its timing (Figs. 3, S3, and S4), thereby circumventing the ‘arms race’. However, this ‘arms race’ observed in synergy B can only persist until a second threshold (red dotted line) is reached, whereby a further increase in muscle activity becomes unsustainable. At this point, the second fast adaptation process (blue arrow i.e., switch-back) is recruited, allowing the monkeys to cease flexing their fingers by excessive activation of synergy B, thus concluding the ‘arms race”. Meanwhile, an alternative, sustainable strategy to perform finger extension has been developed (Fig. 9). Specifically, the monkey increasingly recruited synergy C (wrist flexors, PL and FCR) to aid finger extension using the tenodesis effect (wrist flexion), which was more effective after the ‘arms race’ was concluded. These implications can also be applicable to Monkey B (see Extended result in SI Appendix).

DISCUSSION

In our crossed tendon transfer (TT) model, we identified multiple distinct modes of CNS adaptation, each distinguished by their characteristic time course. Notably, changes involving the relocated muscles (FDS and EDC) and their synergists (synergy A and B) exhibited rapid alterations within a few days, during both the early and later phases of adaptation. We propose that the early changes represent a maladaptive phase, while the later restoration of original patterns, coupled with compensation, might represent the achievement of a 'good enough' functional state. In addition, changes involving certain non-relocated muscles were slower and more gradual throughout the adaptation period, suggesting a compensatory role. These slower adaptations appear to mitigate maladaptive responses and contribute to improved performance after achieving a “good enough” adaptation, possibly through exploitation of an active tenodesis effect. We will first explore the potential causes of this distinct adaptation in relocated versus non-relocated muscles, followed by a discussion on the potential interactions between these different adaptation modes.

519 ***Relocated muscles and their synergists: early and late adaptation***

520 Given the stability of muscle synergy composition (Fig. S7), the CNS adapted to
521 relocated muscles (FDS and EDC) by swapping the temporal activation patterns
522 of the original flexor and extensor synergies, and also their host synergies
523 (synergy A and B). This suggests that selectively altering single muscles within
524 co-activated groups is challenging for the CNS, with much daily muscle activity
525 potentially generated through co-activation modules (Overduin et al., 2008;
526 Berger et al., 2013; Takei et al., 2017; Madarshahian and Latash, 2022). The
527 stable muscle synergy composition after surgery supports modular control via
528 synergies (d'Avella et al., 2003; Bizzi and Cheung, 2013).

529 However, this adherence to established synergy structures created a
530 fundamental conflict following crossed tendon transfer. Activating the original
531 extensor synergy (Synergy B), for instance, now inevitably co-activated the
532 surgically transferred EDC, which functioned mechanically as a flexor (Fig. 6A-D,
533 S7). This highlights a tension between maintaining the integrity of these neural
534 modules and the need for fractionated control – the ability to selectively drive
535 muscles independently – when faced with altered biomechanics. Consequently,

536 the CNS opted to swap temporal activation of the muscle synergy, leaving the
537 synergy itself unchanged.

538

539 The observed initial adaptation, where the temporal activation patterns of the
540 entire flexor and extensor synergies were swapped (Fig. 6E-F, Fig. 7), can be
541 interpreted in light of this tension. Rather than attempting the potentially complex
542 task of fractionating control within the extensor synergy (e.g., activating
543 ED23/ECU without EDC), the CNS appeared to adopt this simpler strategy of
544 repurposing the entire synergy module based on the new primary function of the
545 transferred muscle (EDC as flexor, FDS as extensor). However, this initial
546 adaptation turned out to be maladaptive because this strategy failed functionally
547 due to the unresolved mechanical conflict within the activated synergy (Figs. 4B,
548 8B). It involved muscles unaffected by the TT, leading to a steady increase of
549 antagonistic muscle activity and thus antagonistic proprioceptive feedback in the
550 non-transferred muscles over time.

551

Notably, the maladaptive swapped-activation strategy observed early on was abandoned during the late adaptation phase, with synergy activation patterns reverting towards their original state (Fig. 6, 7). This reversion occurred despite remaining mechanical antagonism, suggesting the CNS did not achieve perfect fine-grained fractionation but instead adopted a different strategy, perhaps driven by the high cost of the internal conflict (Fig. 8B, 'arms race'). This outcome aligns with principles of "good enough" motor control (Mussa-Ivaldi and Bizzi, 1995; Ranganathan et al., 2013; Gijsberts et al., 2014), where functional success and potentially reduced effort are prioritized over perfect efficiency, especially when faced with constraints. Indeed, functional recovery was largely achieved (Fig. 4A) and maladaptive behaviors reduced (Fig. 4B) during this late phase. Crucially, this reversion to the less conflicted original timing was likely enabled only by the concurrent development of slower compensatory strategies, like the tenodesis effect (Fig. 9, discussed below), which provided an alternative means to achieve task goals.

The rapid nature of both the initial synergy swap and the later switch-back—typically stabilizing within days—suggests distinct fast adaptive processes, potentially triggered by strong error signals. The initial maladaptation could

plausibly be linked to the 'sensory surprise' from altered proprioceptive feedback (Kitazawa et al., 1995; Martin et al., 1996; Smith et al., 2006; Edwards et al., 2012; Petitet et al., 2018) driving a rapid but flawed response. While lingering discomfort cannot be fully excluded after the initial recovery period, the specific, evolving nature of the synergy changes over weeks seems primarily attributable to the fundamental sensorimotor disruption itself rather than ongoing pain.

Contextualizing these findings requires considering different forms of plasticity. For instance, while operant conditioning demonstrates that even spinal reflexes can be substantially modified over weeks, primarily through gain modulation within specific pathways (Thompson and Wolpaw, 2014), adapting to the tendon transfer studied here presented a distinct challenge. The drastically altered sensorimotor mapping and mechanics likely necessitated the broader, multi-level network reorganization reflected in our complex multi-timescale findings, rather than primarily tuning an existing response.

586 It is important to note that while our primary analysis focused on muscle synergies
587 during grasping epochs, the tendon transfer also induced significant deficits in
588 the preceding reaching movements (Supplementary Videos S2, S3, S6; Figs. 4B,
589 D), highlighting that adaptation encompassed the entire reach-to-grasp sequence.
590 Although the reach component was not quantitatively analyzed here, its recovery
591 likely interacted strongly with the adaptation of grasp control, given the need to
592 coordinate the full limb trajectory under new mechanical constraints. Furthermore,
593 the development of compensatory strategies, such as the tenodesis effect aiding
594 hand pre-shaping, likely influenced both reach and grasp components.

595

596 ***Slow and gradual adaptation of several non-relocated muscles***

597 The initial maladaptive phase, characterized by swapped synergy activation
598 patterns, coincided with significant functional deficits, including malcoordination
599 and increased task times (Fig. 4; Supplementary Videos S2, S3, S6). In contrast,
600 slower adaptive processes emerged over weeks to months in non-transferred
601 muscles (e.g., FDP, ECR, PL, and FCR in Monkey A, Fig. S4), suggesting
602 compensatory mechanisms.

603 A key compensation was the gradual development of wrist flexion to substitute
604 for reduced finger extension. Specifically, the increased activation of Synergy C
605 (wrist flexors FCR and PL, Fig. 6C) during hand opening and pre-shaping (Figs.
606 S3Q, S and S8C; S3AL and S8E) indicates the monkeys' learned use of the
607 tenodesis effect. This biomechanical coupling, where wrist flexion generates
608 passive finger extension (Zajac, 1992; Cash and Jones, 2011), provided a viable
609 alternative for hand opening, ultimately enabling the 'switch-back' of Synergies A
610 and B and the recovery of task performance (Fig. 4).

611 Additionally, the non-transferred finger flexor FDP showed a slow, gradual
612 increase in activity, independent of its original synergy (Synergy D) (Fig. S4F, P;
613 Fig. S3M). This suggests complex, slow-timescale adjustments, potentially
614 involving altered synergistic relationships or novel independent muscle control.

615

616 ***Neural adaptation from different adaptive modules***

617 A key question concerns the interaction between rapid and gradual adaptation
618 processes. Our model (Fig. 6) proposes that the large initial sensory prediction
619 error (SPE) from the tendon transfer triggered a fast adaptive process – the

observed synergy swap – which, despite being maladaptive, rapidly altered the sensorimotor state. From this altered state, slower processes were subsequently recruited, including both a continued maladaptive strategy (Process A, e.g., the Synergy B 'arms race') and the development of compensatory movements (Process B, e.g., tenodesis via Synergy C). The cumulative cost of the maladaptive process likely triggered a second fast adaptation – the switch-back to the original synergy timing. This final shift was enabled by the compensatory strategy (Process B), resulting in a stable 'good enough' functional outcome despite residual antagonism (Ranganathan et al., 2013). Further understanding requires considering factors not assessed here, such as the roles of spinal reflex pathways (Smith et al., 2006) and fusimotor drive (Vallbo et al., 1979; Hospod et al., 2007).

Implication for sensorimotor rehabilitation

Our findings, revealing distinct phases including initial maladaptation followed by slower compensation and functional recovery, hold potential implications for rehabilitation. A staged approach mirroring these phases could be beneficial: an early phase might focus on minimizing sensory prediction errors and reducing

maladaptive responses through techniques aimed at integrating the altered body schema (e.g., using visual feedback or task-oriented practice with managed error) (Nudo et al., 1996; Takeuchi and Izumi, 2012; Zeiler and Krakauer, 2013; Foell et al., 2014; Levin et al., 2015; De Nunzio et al., 2018; Sattin et al., 2023; van Vliet et al., 2023).

Subsequently, a later phase could employ task-specific training to promote effective compensatory strategies, similar to the slow adaptations observed here. Encouraging functional compensation might facilitate the eventual abandonment of maladaptive patterns and the consolidation of a stable, functional motor strategy, consistent with the eventual recovery observed (Murata et al., 2008).

650 **METHODS**

651 ***Animals***

652 Data were collected using two male macaque monkeys (*Macaca fuscata*; Monkey
653 A: 7.8 kg and Monkey B: 9.9 kg) purpose-bred at the National Bioresource Project
654 (NBRP). They were kept in custom-made primate cages, allowing for potential
655 pair housing. Both monkeys were trained to perform a simple grasping task.
656 During experimental recordings, the monkeys were seated in a primate chair
657 without further restraint. Their head movement remained unrestricted at all times.

658

659 ***Procedures***

660 All procedures were designed to minimize discomfort and pain and approved by
661 the institutional Animal Care and Use Committees at the National Center of
662 Neurology and Psychiatry (NCNP), Tokyo, Japan. Details of the surgical
663 operations, experimental setup, and procedures for electromyography (EMG)
664 recordings have been previously described (Takei and Seki, 2010).

665
666

667 ***EMG implant surgery***

668 Both animals were familiarized with the experimental setup and trained to perform
669 the behavioral task prior to surgery. After an initial training period, EMG
670 electrodes were chronically implanted subcutaneously into several muscles of the
671 left forearm including the FDS, FDP, and EDC (Figs. 1, 3C, and S1C). Individual
672 muscles were localized and confirmed using electrical microstimulation before
673 implanting EMG electrodes chronically by two methods. For muscles involved in
674 the crossed tendon transfer procedure, muscle fascia was cut and EMG wires
675 with looped ends were placed on top of the muscle belly. These were then
676 secured by reclosing the fascia with absorbable suture threaded through the loop
677 (AS-361, stainless-steel Cooner wire, Conner Wire Co., Chatsworth, CA, USA).
678 All other muscles were directly implanted into the muscle belly using a 22-gauge
679 hypodermic needle. Each wire was threaded into the needle tip, folded back along
680 the shaft, and inserted into the muscle before carefully retracting the needle.
681 Electrode separation for bipolar recordings was approximately 5–10 mm. Note
682 that some EMG recording sites were lost over time. Surgical procedures were
683 carried out under deep general anesthesia (sevoflurane 1.5 to 2.5% in 2:1
684 O2/N2O) and with full aseptic precautions. Heart rate, blood pressure, body

685 temperature, and blood oxygen saturation were monitored throughout surgery.
686 Analgesics and antibiotics were administered intramuscularly for at least one
687 week postoperatively.
688

689 ***Tendon-Transfer Surgery***

690 After a minimum four-week recovery period from EMG implant surgery, TT
691 surgery was performed. The FDS and EDC tendons were cut as distally as
692 possible (immediately below and above the wrist for FDS and EDC, respectively)
693 to avoid damaging the Golgi tendon organ located near the junction between the
694 muscle fibers and tendon (Schoultz and Swett, 1972; Jami, 1992). Tendons were
695 then guided either through the gap between the radius and ulnar bone (Monkey
696 A), or around the wrist and then re-attached to the tendon of the antagonist
697 muscle using a tendon graft harvested from the plantaris tendon of the lower limb
698 (Monkey B; EDC → FDS: direct connection; and FDS → EDC: tendon grafting).
699 This was only necessary in Monkey B since the tendons used for the cross-
700 transfer were too short. This surgical procedure aimed to reverse the primary
701 mechanical actions of the manipulated muscles, making the FDS tendon an
702 effective finger extensor and the EDC tendon an effective finger flexor. The

703 success and nature of this mechanical rearrangement were verified post-
704 operatively via direct muscle stimulation (see Methods subsection 'Tendon
705 transfer confirmation' and Fig. 2). The general organization and function of the
706 major forearm muscles involved in finger flexion and extension in *Macaca fuscata*
707 are broadly comparable to those in humans (Vanhoof et al., 2021; Yan et al.,
708 2022).

709 Surgical procedures were carried out under deep general anesthesia
710 (sevoflurane 1.5 to 2.5% in 2:1 O_2/N_2O) and with full aseptic precautions. Heart
711 rate, blood pressure, body temperature, and blood oxygen saturation were
712 monitored throughout surgery. Analgesics and antibiotics were administered
713 intramuscularly for at least one week postoperatively. Both monkeys wore a
714 plaster cast post-surgery, but its effectiveness was limited (lasting approximately
715 one week).

716

717 ***Tendon transfer confirmation***

718 To verify the success and long-term stability of TT surgery, two procedures (Fig.
719 2) were implemented. During the first procedure, the monkey was sedated and

720 its arm was secured to a metal frame (Fig.2A). Electrical stimulation was then
721 applied to either the FDS or EDC muscle (50 mA, DS8R, Digitimer, Welwyn
722 Garden City, UK), while ultrasound scans of tendon movements were
723 concurrently captured (SONIMAGE MX1, Konica Minolta, Inc., Tokyo, Japan
724 (Nordez et al., 2009; Dieterich et al., 2017).

725 Figure 2B shows a sonogram of the FDS muscle and its intramuscular tendons.
726 The left side displays a static image of the FDS muscle at a specific moment, with
727 white arrows indicating the FDS tendon used for measurement. The right side
728 shows staggered images (top white box) of the FDS tendon displacement
729 triggered by muscle stimulation. The lower right inset illustrates the measurement
730 area. The displacement wave area represents the intensity of muscle contraction,
731 and was calculated by measuring the average duration (a, in seconds) and
732 amplitude (b, in cm) of three successive waves. The area (a*b/2) and regression
733 line for FDS (red) and EDC (blue) (R^2 > 0.5 for FDS) for days 0, 7, and 105 post-
734 TT are shown (Fig. 2C). The results suggest that the muscle contractions induced
735 by direct electrical stimulation remained nearly constant.

736 For the second procedure, high-speed videos (37U Series Color Industrial
737 Camera, The Imaging Source, Charlotte, NC, USA) of the monkey's finger
738 movements were recorded while electrically stimulating the FDS or EDC. Markers
739 were placed on the nails of the index, middle, and ring fingers (Fig. 2A) to
740 measure finger displacement in xyz-dimensions using DeepLabCut software
741 (Mathis et al., 2018; Nath et al., 2019). The sum of Euclidean distances of each
742 marker from the origin of the three-dimensional (3D) coordinate system was
743 computed as a scalar quantity. Post-surgery, movement along the z-axis
744 reversed, indicating a shift from finger flexion to extension due to TT (Fig. 2D;
745 blue: pre-TT on surgery day, dark brown: post-TT on surgery day, light brown: 1
746 wk post-TT, and red: 3 wk post-TT). The scalar quantities of each finger did not
747 significantly change during muscle stimulation on days 0-, 7-, and 105-days post-
748 TT (Fig. 2E), suggesting there was no postoperative tendon rupture or slackening.

749

750 ***Data recordings***

751 EMG signals were recorded using the AlphaLab SnR system (Alpha Omega
752 Engineering, Hamerkava St. 6, Ziporit Industrial Zone, P.O.Box 810, Nof HaGalil

(Nazareth Illit) 1789062, Israel), displayed online and then stored on a hard drive for later off-line analysis using MATLAB (MathWorks, Natick, MA, USA). Data were recorded at 11 kHz and processed for analysis as follows. 1. Down-sampled to 5 kHz; 2. 50 Hz high-pass filtered (6th order Butterworth filter); 3. rectified; 4. 20 Hz low-pass filtered (6th order Butterworth filter); and 5. down-sampled to 100 Hz. Behavioral task events were recorded as transistor–transistor logic (TTL) signals using the AlphaLab SnR system. Monkey behavior was further recorded by two cameras (Sanyo VPC-WH1, 60 fps [Sanyo, Osaka, Japan]; and Casio EX-100F, 240 fps [Casio, Tokyo, Japan] for monkeys A and B, respectively) from two different angles (top and side view). The images were later used to detect additional behavioral events (contact time with the object and pull onset for Monkey A; and food touch and food lift onset for Monkey B), and detection of possible changes in the animal's general movement pattern. Kinovea software was used for this video analysis (free and open-source software; https://www.kinovea.org/).

771 ***Behavioral task***

772 Before and after EMG surgery, the monkeys were trained on a simple grasping
773 task that involved a small object attached to a rod (Fig. 3B for Monkey A; and Fig.
774 S1B for Monkey B). For Monkey A, object 1 was a small rod placed between two
775 side walls encouraging the monkey to grasp the rod with a precision grip using
776 the tips of the index finger and thumb (controlled grasp). The force used to
777 compress the spring while pulling was low and the distance moved short. Object
778 2 had to be grasped in the same way. However, the force to compress the spring
779 was higher and the distance moved longer (object 1: 300 cN, 4 mm; and object
780 2: 800 cN, 30 mm). The monkey was asked to grasp and hold the objects for
781 approximately 300–500 ms (Fig. 3A–D). After completing the trial, the monkey
782 was rewarded with a piece of fruit that had to be taken from the experimenter's
783 palm. The task sequence for Monkey A ranged from object 1 hold onset to object
784 2 hold offset (Fig. 3C, D; and 'Data Analysis' below). For Monkey B, object 1 was
785 a small rod that was grasped and pulled (300 cN, 4 mm) using a lateral
786 prehension grip (like using a door key), and resembling a power grip rather than
787 a natural grasp. However, instead of grasping object 2, Monkey B picked up a
788 piece of fruit from an allocated location. In doing so, the monkey had to cross the

789 path of a photo cell which was detected by the recording system (Fig. S1A–D).
790 The task sequence to be analyzed for Monkey B ranged from object 1 hold onset
791 to food touch, which was indicated by a LED (Fig. S1C, D; and 'Data Analysis'
792 below).

793 For Monkey A, the task sequence was as follows (Fig. 3A; and Supplementary
794 Video S1). From a starting position in front of the monkey, it had to lift its arm and
795 move towards object 1, grasp, pull, and then hold the object for 500 ms.
796 Immediately after releasing object 1, Monkey A proceeded to move its hand
797 towards object 2, which was located to the right of object 1. Again, the monkey
798 had to grasp, pull, and then hold the object for another 500 ms. Each hold period
799 was accompanied by an audio signal which stopped once the hold duration was
800 sufficient. After completing the task, which was signaled by another acoustic
801 signal, the monkey was rewarded with a piece of fruit presented by the
802 experimenter and taken by the monkey.

803 For Monkey B, the first part of the sequence was identical. However, after
804 releasing object 1, Monkey B was required to pick up a piece of fruit from an
805 allocated location (Fig. S1A, B; and Supplementary Video S5). In doing so, the

806 monkey passed a photocell in front of the food well. This event was detected by
807 the recording system and a video camera (a red LED triggered by activation of
808 the photocell). For the analysis, only object 1 and the food grasp were considered
809 in monkeys A and B, respectively.

810

811 ***Data analysis***

812 *EMG analysis*

813 EMG data were normalized to the average time for each monkey to complete a
814 trial (object 1 hold onset ➔ object 2 hold offset/LED offset = 100%). Data were
815 cropped and aligned according to the time stamps (Obj1 hold offset ± 15%; and
816 LED onset [food touch] ± 15% for monkeys A and B, respectively). Recorded
817 EMGs from the pre- and post-tendon surgery period were averaged for each
818 recording and compared over experimental sessions. For both monkeys, the
819 muscles used for EMG analysis were: FDS and EDC for pre- (control) and EDC
820 for post-TT (experimental).

821 Both monkeys required time to recover from surgery. Once they were able to
822 perform the task on their own, data collection started (29 and 20 days post-
823 surgery for monkeys A and B, respectively). After tendon surgery, EMG signals
824 for FDS, FCU, and FCR deteriorated in Monkey B. Therefore, there is no
825 experimental data for these muscles in this monkey and they were excluded from
826 the muscle synergy analysis.

827

828 *Synergy analysis*

829 The EMG envelopes obtained from pre-processing raw EMG data were divided
830 by the mean value to normalize activity. Muscle synergies were then extracted
831 for each session using NMF (d'Avella et al., 2003). NMF decomposes the EMG
832 data matrix M, as a product of two matrices C and W:

833 $$M = CW^T + re = \Sigma c_i {w_i}^T + re$$

834 where the vector wi and column of matrix W are muscle synergies; the vector ci,
835 and column of matrix C are their temporal coefficients; and re represents the
836 residuals. Multiplicative update rules were used for decomposition (Lee and

837 Seung, 1999). Updating matrices for decomposition from 20 different random
838 initial matrices was started, and factorization results with least residuals among
839 the 20 results were used. To improve robustness of the muscle synergies, one
840 set of muscle synergies was extracted from EMG data of multiple trials of each
841 day. A k-fold cross validation was used, with k = 4 i.e., EMG data set of multiple
842 trials during the day was split into four data sets, in which three data sets were
843 for training and one data set was for testing. Synergy matrix W was calculated
844 from three training data sets using NMF, and then a coefficient matrix C was
845 calculated by decomposing the EMG matrix M of the test data set with a fixed W
846 matrix of the training data set. This operation was repeated by changing the test
847 data set for each four data sets. Finally, the extracted four C matrices and four W
848 matrices were averaged to obtain daily synergies.

849 The number of synergies was determined as the number where VAF exceeded
850 a threshold. This threshold was set as 0.8. To clarify the effect of TT, the number
851 of synergies for each monkey was determined, assuming that trial-by-trial
852 variation in synergies within the same monkey was small. MATLAB 'nnmf'
853 function was used for NMF.

854

855 To determine whether the weights of muscle synergies changed after TT, the
856 following procedure was used. First, the average of each pre-TT spatial synergy
857 was calculated and used as control data to calculate the cosine distance for all
858 post-TT spatial synergies. This generated four distance relationships for each
859 pre-TT synergy. If the change in spatial synergy before and after TT was small,
860 then only one of the four cosine distances (e.g., synergy A before TT and synergy
861 A after TT) should be significantly smaller. Two-way ANOVA was conducted
862 using the type of synergy and session as factors for the cosine distance. The
863 significance of synergy pairs was identified using the Bonferroni post-hoc test.
864

865 *Cross-correlation analysis*

866 Cross-correlation analysis was performed to examine pre- and post-surgery EMG
867 signals as well as temporal activation coefficients of extracted muscle synergies.
868 Cross-correlation coefficients were calculated using MATLAB (MathWorks,
869 corrcoef.m function). These were plotted for different muscles and muscle
870 synergy activation coefficients over experimental sessions for comparison.

871 Based on cross-correlation analysis, five ‘landmark days’ were identified for
872 further analysis (Figs. 2G, H, and S2D). These days represent distinct stages in
873 the recovery process and excluded pre-surgery control data. The first landmark
874 day was chosen from one of the initial recording sessions after TT surgery (days
875 29 and 22 in monkeys A and B, respectively) when the cross-correlation
876 coefficients had changed significantly compared with control data. The second
877 day was then chosen from a time period just before the switch-back, when the
878 cross-correlation coefficients had started to return to their original values (days
879 64 and 36). Another day was then picked from the period when the coefficients
880 were still changing significantly (days 69 and 44) and before starting to saturate.
881 At this point the next day was defined (days 79 and 48). Finally, the final landmark
882 day was chosen from one of the last recording sessions when the behavior had
883 fully recovered (days 99 and day 64 for monkeys A and B, respectively).

884

885 *Behavioral analysis*

886 To examine behavioral recovery, the duration, onset, and offset of object and
887 food grasps were analyzed. Event times extracted from the video analysis were
888 used for alignment of EMG data and subsequent cross-correlation and synergy

analyses, along with recorded event TTL signals. For each experimental session, the first 20 trials of each video recording were analyzed. In Monkey A, the following events were detected and in-between times stored in ms: touch onset, pull onset, and hold onset (resulting in grasp duration and pull time) for object 1 and object 2. In Monkey B, the following events were detected and in-between times stored: touch onset, pull onset, and hold onset (resulting in grasp duration and pull time) for object 1; and for the food grasp component of the task, LED onset, food-touch onset, food-lift onset, LED offset, and movement end (contact of food with mouth).

Contact times (touch onset ➔ pull onset) for Monkey A were plotted in ms (mean ± SD) over number of days from tendon surgery for object 1. For Monkey B, contact times with food (food-touch ➔ food-lift onset) were plotted in ms (mean ± SD).

ANOVA was performed to compare control data recorded before and after tendon surgery. In total, 5 and 3 control sessions vs. 35 and 22 experimental sessions were used for analyses in monkeys A and B, respectively.

To quantify the observed malcoordinated reaching behavior, video footage was analyzed and the means of 10 consecutive trials calculated for each session as follows. For Monkey A, time spent within a specific spatial window covering the area behind and between the two objects was measured; the monkey passed through this space almost exclusively while exhibiting the impairment (see Fig. 3E, crossing of the yellow dotted line). In Monkey B, the time spent in contact with the rear plate of the object was measured (see Fig. S1G).

Joint kinematics analysis

To determine whether compensatory movements occurred, steady state changes in joint angles were examined before and after recovery. Using DeepLabCut (Mathis et al., 2018; Nath et al., 2019), key points on the fingers and wrists were tracked from experimental videos. From the obtained key points, the vector v_1 connecting the wrist and fingers and vector v_2 connecting the arm and wrist were estimated. The joint angle θ was calculated as follows:

$$cos(\Theta) = \frac{\underline{v}_2 \cdot \underline{v}_3}{|\underline{v}_2|\,|\underline{v}_3|} \rightarrow \Theta = cos^{-1}\left(\frac{\underline{v}_2 \cdot \underline{v}_3}{|\underline{v}_2|\,|\underline{v}_3|}\right)$$

DATA, MATERIALS, AND SOFTWARE AVAILABILITY

Matlab scripts and raw data will be made available online. All study data are included in the article and/or SI Appendix.

ACKNOWLEDGEMENTS:

We would like to express our sincere gratitude to Drs. Francisco Valero-Cuevas and Andrea d'Avella for their invaluable comments and constructive suggestions on the earlier version of the manuscript, and Drs Nicholas Schweighofer and Gerald E. Loeb for stimulating discussion. We would also like to thank Dr. Naomichi Ogihara and Prof. Toshiyasu Nakamura for their valuable insights and technical advice on tendon surgery in the hand and forearm of primates. We are grateful to Drs. Kumiko Oida and Chika Sasaki for their medical care of the experimental animals, vital help during surgery, and training of the animals. Lastly, we would like to thank Masahi Koizumi for designing parts of the experimental setup and Drs. Joachim Confais, Shinji Kubota, Saeka Tomatsu, Tatsuya Umeda, and Natsumi Uchida for their support and assistance during the proceeding pilot study. We thank Rachel James, PhD, from Edanz (https://jp.edanz.com/ac) for editing a draft of this manuscript.

This work was supported by Grants-in-Aid for Scientific Research from the Ministry of Education, Culture, Sports, Science, and Technology of Japan (26120003, 26250013, 15K21754, 19H05724, 19H01092, 23H05488, and 24K21313), the Japan Agency for Medical Research and Development

(JP24gm0010009), the Japan Science Technology Agency Precursory Research for Embryonic Science and Technology program, commissioned research (no. 22102) from the National Institute of Information and Communications Technology, and commissioned research by National Institute of Information and Communications Technology (NICT), Japan (all to K.S.). This work is also supported in part by the NSF CRCNS Japan-US 2113096 to K.S. (Subaward PI) and Francisco Valero-Cueva (PI). The content is solely the responsibility of the authors and does not necessarily represent the official views of the NSF.

REFERENCES

Berger DJ, Gentner R, Edmunds T, Pai DK, d'Avella A (2013) Differences in Adaptation Rates after Virtual Surgeries Provide Direct Evidence for Modularity. The Journal of Neuroscience 33:12384-12394.

Bizzi E, Cheung VC (2013) The neural origin of muscle synergies. Frontiers in Computational Neuroscience Volume 7 - 2013.

Bowlus TH, Lane RD, Stojic AS, Johnston M, Pluto CP, Chan M, Chiaia NL, Rhoades RW (2003) Comparison of reorganization of the somatosensory system in rats that sustained forelimb removal as neonates and as adults. J Comp Neurol 465:335-348.

Cash DJW, Jones JWM (2011) The role of tenodesis in surgery of the upper limb. The Journal of Bone & Joint Surgery British Volume 93-B:285-292.

Cheung VC, Turolla A, Agostini M, Silvoni S, Bennis C, Kasi P, Paganoni S, Bonato P, Bizzi E (2012) Muscle synergy patterns as physiological markers of motor cortical damage. Proc Natl Acad Sci U S A 109:14652-14656.

d'Avella A, Saltiel P, Bizzi E (2003) Combinations of muscle synergies in the construction of a natural motor behavior. Nature Neuroscience 6:300-308.

Davidson PR, Wolpert DM (2003) Motor learning and prediction in a variable environment. Curr Opin Neurobiol 13:232-237.

De Nunzio AM, Schweisfurth MA, Ge N, Falla D, Hahne J, Gödecke K, Petzke F, Siebertz M, Dechent P, Weiss T, Flor H, Graimann B, Aszmann OC, Farina D (2018) Relieving phantom limb pain with multimodal sensory-motor training. J Neural Eng 15:066022.

Dieterich AV, Botter A, Vieira TM, Peolsson A, Petzke F, Davey P, Falla D (2017) Spatial variation and inconsistency between estimates of onset of muscle activation from EMG and ultrasound. Sci Rep 7:42011.

Edwards MJ, Adams RA, Brown H, Pareés I, Friston KJ (2012) A Bayesian account of 'hysteria'. Brain 135:3495-3512.

Fleury L, Prablanc C, Priot AE (2019) Do prism and other adaptation paradigms really measure the same processes? Cortex 119:480-496.

Foell J, Bekrater-Bodmann R, Diers M, Flor H (2014) Mirror therapy for phantom limb pain: brain changes and the role of body representation. Eur J Pain 18:729-739.

Gaetz W, Dockstader C, Furlong PL, Amaral S, Vossough A, Schwartz ES, Roberts TPL, Scott Levin L (2023) Somatosensory and motor representations following bilateral transplants of the hands: A 6-year longitudinal case report on the first pediatric bilateral hand transplant patient. Brain Res 1804:148262.

Gijsberts A, Bohra R, Sierra González D, Werner A, Nowak M, Caputo B, Roa MA, Castellini C

(2014) Stable myoelectric control of a hand prosthesis using non-linear incremental learning. Front Neurorobot 8:8.

Green HJ (1997) Mechanisms of muscle fatigue in intense exercise. J Sports Sci 15:247-256.

Hospod V, Aimonetti J-M, Roll J-P, Ribot-Ciscar E (2007) Changes in Human Muscle Spindle Sensitivity during a Proprioceptive Attention Task. The Journal of Neuroscience 27:5172-5178.

Imamizu H, Miyauchi S, Tamada T, Sasaki Y, Takino R, Pütz B, Yoshioka T, Kawato M (2000) Human cerebellar activity reflecting an acquired internal model of a new tool. Nature 403:192-195.

Jami L (1992) Golgi tendon organs in mammalian skeletal muscle: functional properties and central actions. Physiol Rev 72:623-666.

Kitazawa S, Kohno T, Uka T (1995) Effects of delayed visual information on the rate and amount of prism adaptation in the human. J Neurosci 15:7644-7652.

Lee DD, Seung HS (1999) Learning the parts of objects by non-negative matrix factorization. Nature 401:788-791.

Levin MF, Weiss PL, Keshner EA (2015) Emergence of virtual reality as a tool for upper limb rehabilitation: incorporation of motor control and motor learning principles. Phys Ther 95:415-425.

Loeb GE (1999) Asymmetry of hindlimb muscle activity and cutaneous reflexes after tendon transfers in kittens. J Neurophysiol 82:3392-3405.

Luauté J, Schwartz S, Rossetti Y, Spiridon M, Rode G, Boisson D, Vuilleumier P (2009) Dynamic changes in brain activity during prism adaptation. J Neurosci 29:169-178.

Madarshahian S, Latash ML (2022) Reciprocal and coactivation commands at the level of individual motor units in an extrinsic finger flexor-extensor muscle pair. Exp Brain Res 240:321-340.

Martin TA, Keating JG, Goodkin HP, Bastian AJ, Thach WT (1996) Throwing while looking through prisms. II. Specificity and storage of multiple gaze-throw calibrations. Brain 119 (Pt 4):1199-1211.

Mathis A, Mamidanna P, Cury KM, Abe T, Murthy VN, Mathis MW, Bethge M (2018) DeepLabCut: markerless pose estimation of user-defined body parts with deep learning. Nature Neuroscience 21:1281-1289.

Murata Y, Higo N, Oishi T, Yamashita A, Matsuda K, Hayashi M, Yamane S (2008) Effects of motor training on the recovery of manual dexterity after primary motor cortex lesion in macaque monkeys. J Neurophysiol 99:773-786.

Mussa-Ivaldi FA, Bizzi E (1995) The Modular Organization of Motor Control: What Frogs Can Teach Us About Adaptive Learning. IFAC Proceedings Volumes 28:413-418.

Nath T, Mathis A, Chen AC, Patel A, Bethge M, Mathis MW (2019) Using DeepLabCut for 3D markerless pose estimation across species and behaviors. Nature Protocols 14:2152-2176.

Nordez A, Gallot T, Catheline S, Guével A, Cornu C, Hug F (2009) Electromechanical delay revisited using very high frame rate ultrasound. J Appl Physiol (1985) 106:1970-1975.

Nudo RJ, Wise BM, SiFuentes F, Milliken GW (1996) Neural substrates for the effects of rehabilitative training on motor recovery after ischemic infarct. Science 272:1791-1794.

Overduin SA, d'Avella A, Roh J, Bizzi E (2008) Modulation of Muscle Synergy Recruitment in Primate Grasping. The Journal of Neuroscience 28:880-892.

Petitet P, O'Reilly JX, O'Shea J (2018) Towards a neuro-computational account of prism adaptation. Neuropsychologia 115:188-203.

Power JD, Schlaggar BL (2017) Neural plasticity across the lifespan. Wiley Interdiscip Rev Dev Biol 6.

Ranganathan R, Adewuyi A, Mussa-Ivaldi FA (2013) Learning to be lazy: exploiting redundancy in a novel task to minimize movement-related effort. J Neurosci 33:2754-2760.

Sattin D, Parma C, Lunetta C, Zulueta A, Lanzone J, Giani L, Vassallo M, Picozzi M, Parati EA (2023) An Overview of the Body Schema and Body Image: Theoretical Models, Methodological Settings and Pitfalls for Rehabilitation of Persons with Neurological Disorders. Brain Sci 13.

Schärli A, Hecht H, Mast FW, Hossner EJ (2024) How spotting technique affects dizziness and postural stability after full-body rotations in dancers. Hum Mov Sci 95:103211.

Schoultz TW, Swett JE (1972) The fine structure of the Golgi tendon organ. J Neurocytol 1:1-26.

Slawinska U, Kasicki S (2002) Altered Electromyographic Activity Pattern of Rat Soleus Muscle Transposed into the Bed of Antagonist Muscle. The Journal of Neuroscience 22:5808-5812.

Smith MA, Ghazizadeh A, Shadmehr R (2006) Interacting adaptive processes with different timescales underlie short-term motor learning. PLoS Biol 4:e179.

Sperry RW (1940) The functional results of muscle transposition in the hind limb of the rat. Journal of Comparative Neurology 73:379-404.

Sperry RW (1942) Transplantation of motor nerves and muscles in the forelimb of the rat. Journal of Comparative Neurology 76.

Sugita Y (1996) Global plasticity in adult visual cortex following reversal of visual input. Nature 380:523-526.

Takei T, Seki K (2010) Spinal interneurons facilitate coactivation of hand muscles during a precision grip task in monkeys. J Neurosci 30:17041-17050.

Takei T, Confais J, Tomatsu S, Oya T, Seki K (2017) Neural basis for hand muscle synergies in

the primate spinal cord. Proceedings of the National Academy of Sciences 114:8643-8648.

Takeuchi N, Izumi S (2012) Maladaptive plasticity for motor recovery after stroke: mechanisms and approaches. Neural Plast 2012:359728.

Thompson AK, Wolpaw JR (2014) Operant conditioning of spinal reflexes: from basic science to clinical therapy. Front Integr Neurosci 8:25.

Vallbo AB, Hagbarth KE, Torebjörk HE, Wallin BG (1979) Somatosensory, proprioceptive, and sympathetic activity in human peripheral nerves. Physiol Rev 59:919-957.

van Vliet P, Carey LM, Turton A, Kwakkel G, Palazzi K, Oldmeadow C, Searles A, Lavis H, Middleton S, Galloway M, Dimech-Betancourt B, O'Keefe S, Tavener M (2023) Task-specific training versus usual care to improve upper limb function after stroke: the "Task-AT Home" randomised controlled trial protocol. Frontiers in Neurology 14.

Vanhoof MJM, van Leeuwen T, Galletta L, Vereecke EE (2021) The forearm and hand musculature of semi-terrestrial rhesus macaques (Macaca mulatta) and arboreal gibbons (fam.Hylobatidae). Part II. Quantitative analysis. Journal of Anatomy 238:321-337.

Walker JG, Jackson HJ, Littlejohn GO (2004) Models of adjustment to chronic illness: using the example of rheumatoid arthritis. Clin Psychol Rev 24:461-488.

Wester K, Hove LM, Barndon R, Craven AR, Hugdahl K (2018) Cortical Plasticity After Surgical Tendon Transfer in Tetraplegics. Front Hum Neurosci 12:234.

Yan Y, Sobinov AR, Bensmaia SJ (2022) Prehension kinematics in humans and macaques. J Neurophysiol 127:1669-1678.

Yumiya H, Larsen KD, Asanuma H (1979) Motor readjustment and input-output relationship of motor cortex following cross-connection of forearm muscles in cats. Brain Research 177:566-570.

Zajac FE (1992) How musculotendon architecture and joint geometry affect the capacity of muscles to move and exert force on objects: a review with application to arm and forearm tendon transfer design. J Hand Surg Am 17:799-804.

Zeiler SR, Krakauer JW (2013) The interaction between training and plasticity in the poststroke brain. Curr Opin Neurol 26:609-616.

Zemková E (2022) Physiological Mechanisms of Exercise and Its Effects on Postural Sway: Does Sport Make a Difference? Front Physiol 13:792875.

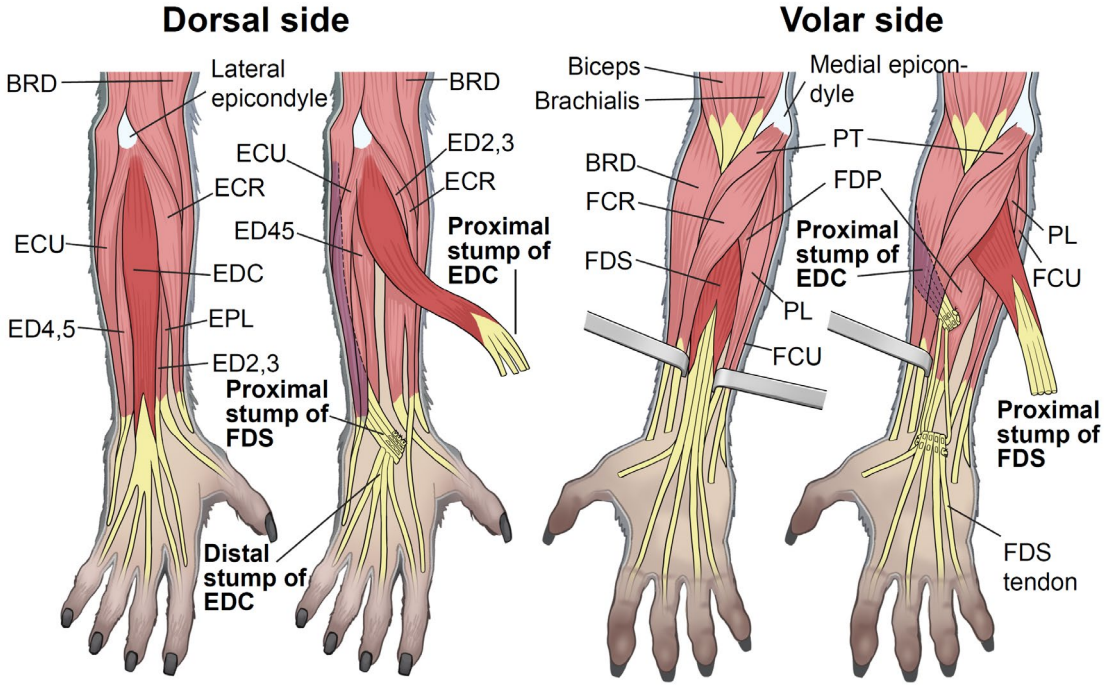

Fig.1: Muscle anatomy of the forearm of the macaque monkey and surgical procedure.

All muscles implanted with electromyography electrodes are labeled. Muscle abbreviations (Monkey A): brachioradialis (BRD), extensor carpi radialis (ECR), extensor carpi ulnaris (ECU), extensor digitorum-2,3 (ED23), extensor digitorum communis (EDC), flexor carpi radialis (FCR), flexor carpi ulnaris (FCU), flexor digitorum profundus (FDP), flexor digitorum superficialis (FDS), and palmaris longus (PL). Additionally implanted muscles in Monkey B: deltoid (DEL) and extensor digitorum-4,5 (ED45). Tendons of EDC and FDS muscles were cross-transferred.

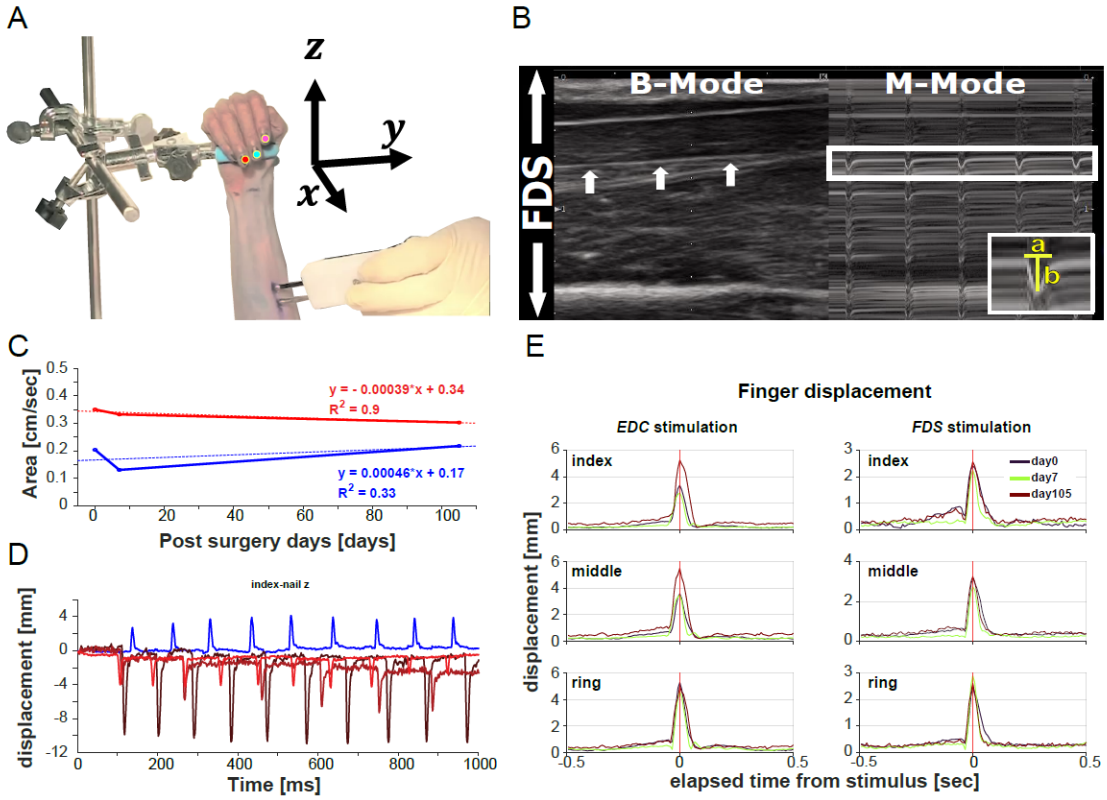

Fig. 2. ***Long term confirmation of tendon surgery effectiveness to alter mechanical properties.***

*(A) Set-up for the ultrasound measurement and video recordings of the stimulation induced movements of the EDC and FDS tendons. (B) Sonogram of the FDS muscle and its intramuscular tendons. Left side (B-mode, i.e., brightness mode) shows the still image of the monkeys forearm at a given point in time. Right side (M-mode, i.e., motion mode) shows the stagged images of the FDS tendon displacement induced by muscle stimulation (50mA). White arrows demarcate the FDS tendon which was used for the measurement. Grayscale gradations correspond to tissue densities: hyperechoic regions (white) denote denser structures like surface of bones and tendons, while hypoechoic areas (black) signify less dense tissues such as adipose tissue and musculature. Inset demonstrates the area measurement. The area of the displacement waves was measured in the M-mode, representing the strength of muscle contraction. We measured the duration (a, sec) and amplitude (b, cm) of three waves and calculated the average. Area = a*b/2(cm/sec) for days 0, 7 and 105 after tendon transfer. (C) Areas under the wave measured in the M-mode for 3 experimental days (0, 7 and 105 days post-TT) and regression lines in red and blue for FDS*

and EDC, respectively. R2>0.5 for FDS. The data suggested that muscle contractions induced by direct electrical stimulation were nearly constant. (D) Markers placed on the index, middle and ring finger nails (A) were used to measure finger displacement in xyz-dimensions. We calculated the sum of the Euclidean distances of each marker from the origin of the 3D coordinate system as a scalar quantity. Observing the movement along the Z-axis, it became reversed post-surgery indicating a reversal from finger flexion to extension due to tendon transfer (D, blue = pre-TT at surgery day; dark brown = post-TT at surgery day; light brown = 1wk post-TT; red = 3wks post-TT). The scalar quantity of the fingers during muscle stimulation did not change much at day 0, 7 and 105 days (E), suggesting that there was no tendon rupture or slackening of the tendons postoperatively (EDC stimulation, left; FDS stimulation, right).

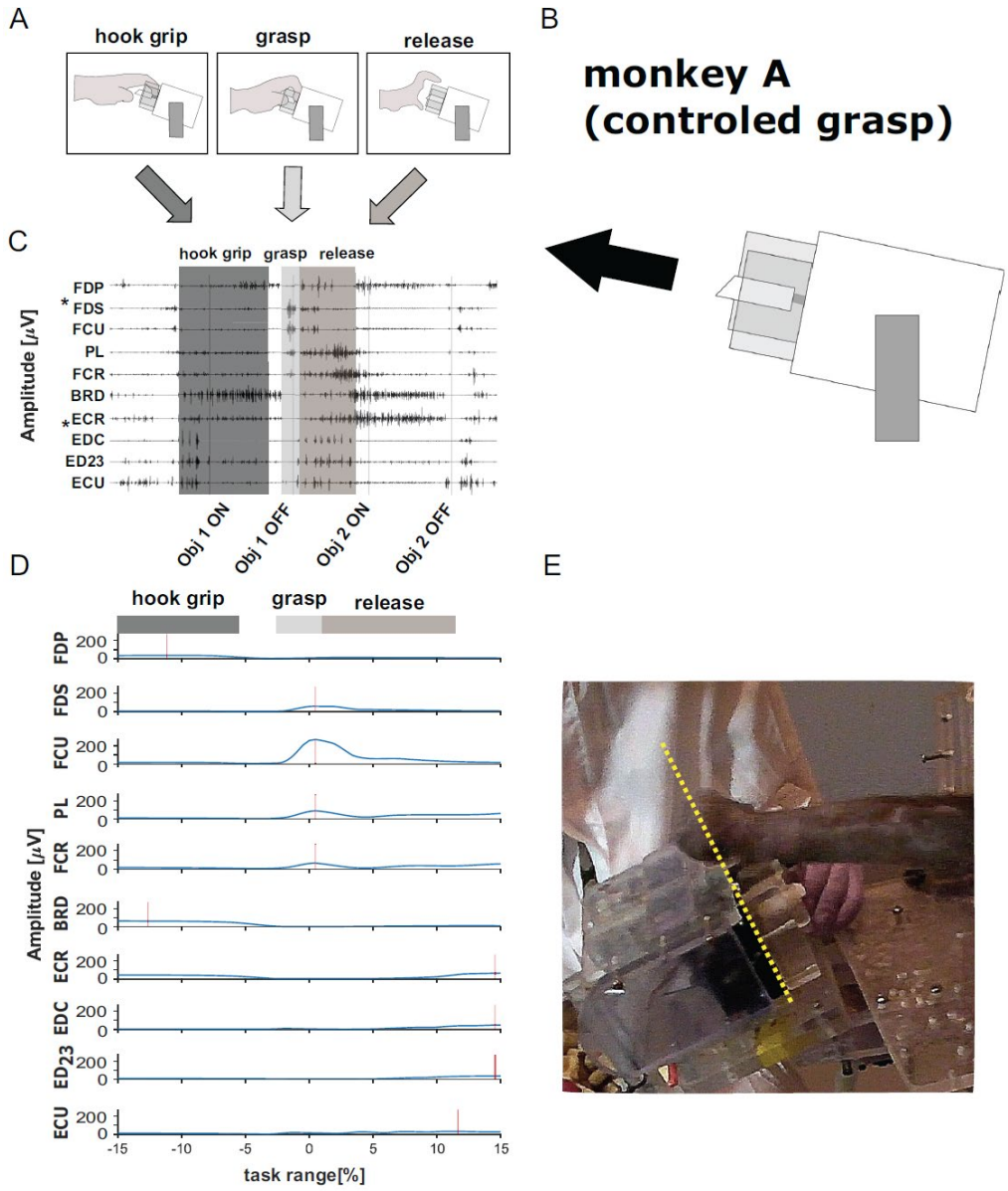

Fig. 3. ***Experimental set-up, task sequence and typical EMG (monkey A).***

(A) Schematic of the behavioral sequence (hook → grasp → release). (B) Schematic of the task object using a rod requiring monkey A to perform a controlled grasp. (C) Typical EMG traces of a control session (high-pass filtered) for all recorded muscles. Gray boxes represent the task sequence. Obj 1 ON: start of the hold period of object 1. Obj 1 OFF: end of the hold period of object 1, i.e., object release. Obj 2 ON: start of the hold period of object 2. Obj 2 OFF: end of the hold period of object 2, i.e., object release. Muscle abbreviations: Brachioradialis (BRD), Extensor Carpi Radialis (ECR), Extensor Carpi Ulnaris

*(ECU), Extensor Digitorum-2,3 (ED23), Extensor Digitorum Communis (*EDC), Flexor Carpi Radialis (FCR), Flexor Carpi Ulnaris (FCU), Flexor Digitorum Profundus (FDP), Flexor Digitorum Superficialis (*FDS), Palmaris Longus (PL). Tendons of the muscles marked with * were cross-transferred. (D) Rectified and smoothed EMG for all recorded muscles (average for one recording session; amplitude [μV] over task sequence [%]). Horizontal bars illustrate the corresponding behavioral periods, red vertical lines indicate peak amplitude for each muscle). (E) The time the monkey spent on the left side of the yellow dotted line while moving from object 1 to object 2 was measured and used to quantify the mal-adaptive behavior.*

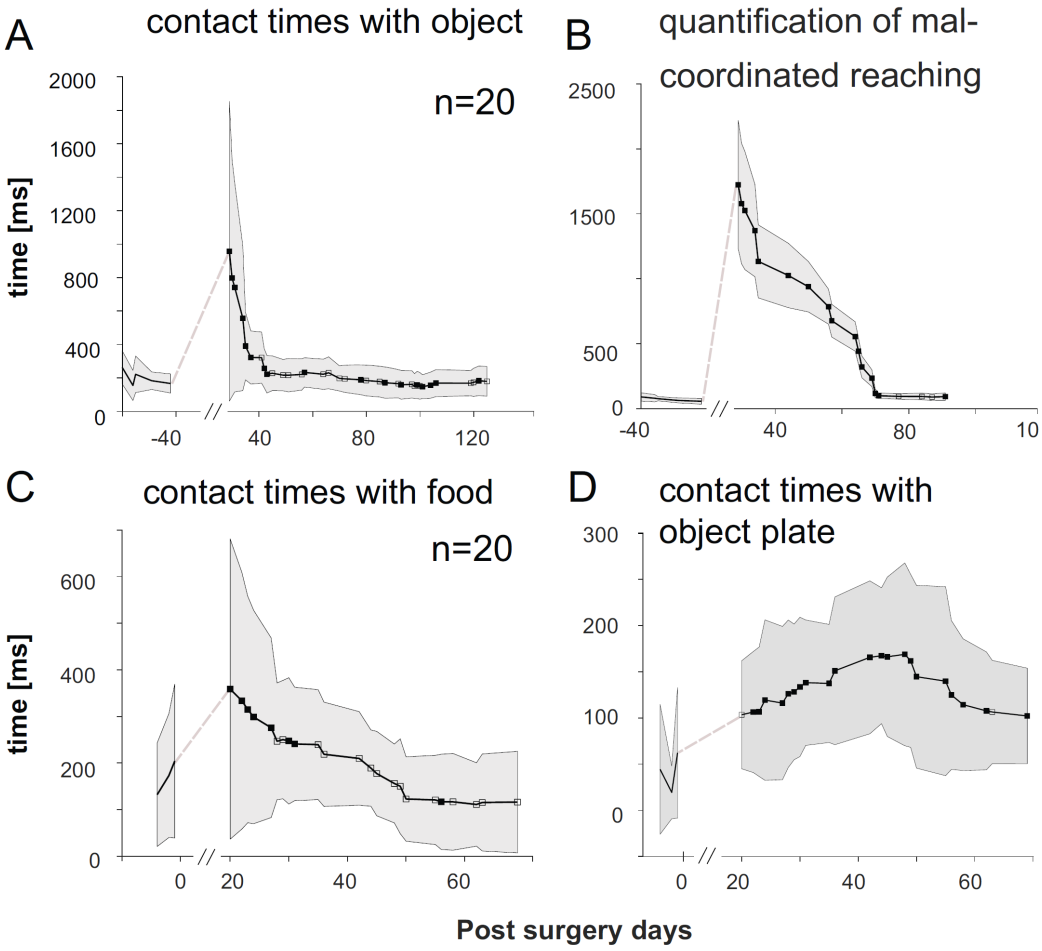

Fig. 4. ***Behavioral analysis and mal-adaptation (monkey A)***

Monkey A: (A) Contact times [ms] with the object for the controlled grasp. (B) Quantification of mal-coordinated behavior. Plotted is the duration [ms] the monkey spent on the left side of the yellow dotted line while moving from object 1 to object 2 (see Fig. 3 E). Monkey B: (C) Contact times with food [ms] during the natural grasp. Each data point represents the average of 20 observations (±SD envelope) plotted in milliseconds over days with respect to TT (day 0). Open squares: n.s., filled squares: $p<0.05$, two-sample t-test. (D) Contact times [ms] with the object plate used to quantify the mal-coordinated reaching behavior. Each data point represents the average of 10 observations (±SD envelope) plotted over days with respect to TT (day 0). Open circles: n.s., filled circles: $p<0.05$, two-sample t-test.

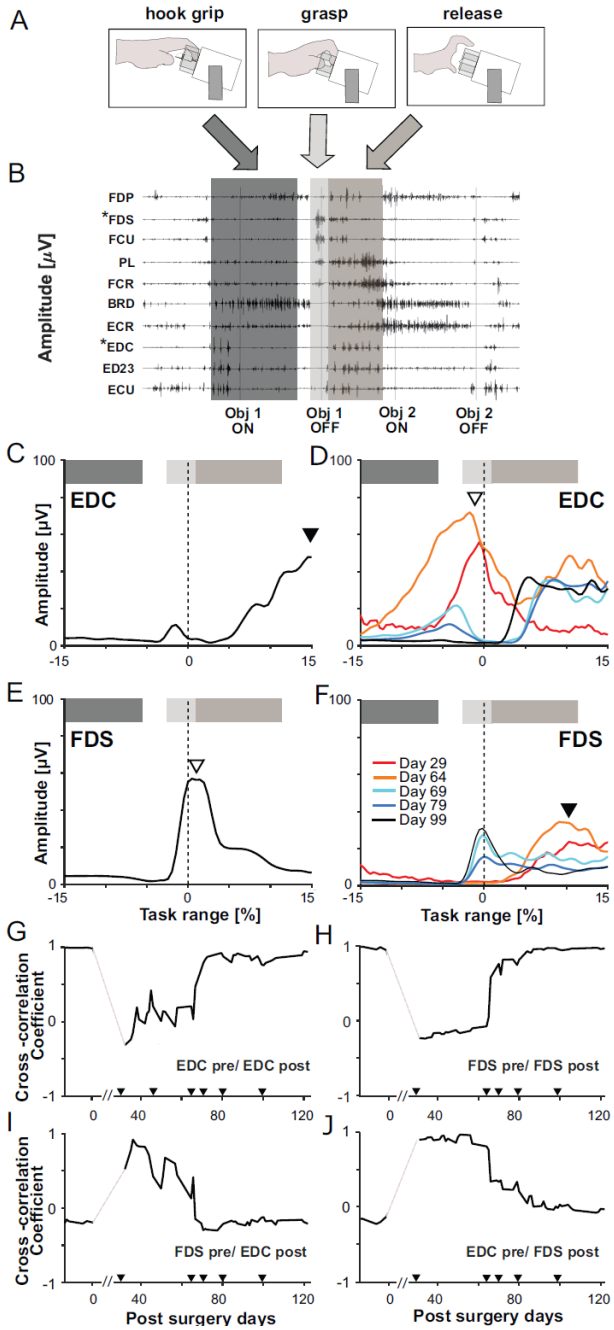

Fig. 5: Task sequence, typical electromyography, ***EMG activity profiles of 'Landmark days' and Cross-correlation coefficients of transferred muscles for all recording sessions (monkey A).***

(A) Schematic of the behavioral sequence (hook → grasp → release). (B) Typical electromyography (EMG) traces of a control session (high-pass filtered) for all recorded muscles. Gray boxes represent the task sequence. Obj 1 ON: start of hold period of object 1; Obj 1 OFF: end of hold period of object 1 (i.e., object release); Obj 2 ON: start of hold period of object 2; Obj 2 OFF: end of hold period

of object 2 (i.e., object release). Tendons of muscles marked * were cross-transferred. (C, D) Electromyography (EMG) activity profiles (μV) for selected 'landmark days' pre- and post-tendon transfer (TT) of extensor digitorum communis (EDC) (C and D, respectively) in Monkey A. Profiles are aligned on hold off-set (object 1) at 0% task range (vertical dashed lines). Horizontal gray bars indicate three behavioral periods: hook, grasp, and release. (E, F) As above but for flexor digitorum superficialis (FDS). Filled triangles in (C) and (F) indicate maximum EMG amplitudes for EDC before TT and FDS (during extension) immediately after TT. Open triangles indicate maximum EMG amplitudes of FDS before and EDC immediately after TT (E and D, respectively). (G–J) Cross-correlation coefficients plotted over experimental days with respect to tendon surgery. G: EDC pre/post; H: FDS pre/post; I: FDS pre/EDC post; and J: EDC pre/FDS post. Dashed lines indicate recovery periods with no recordings. Small triangles (G–J) indicate landmark days.

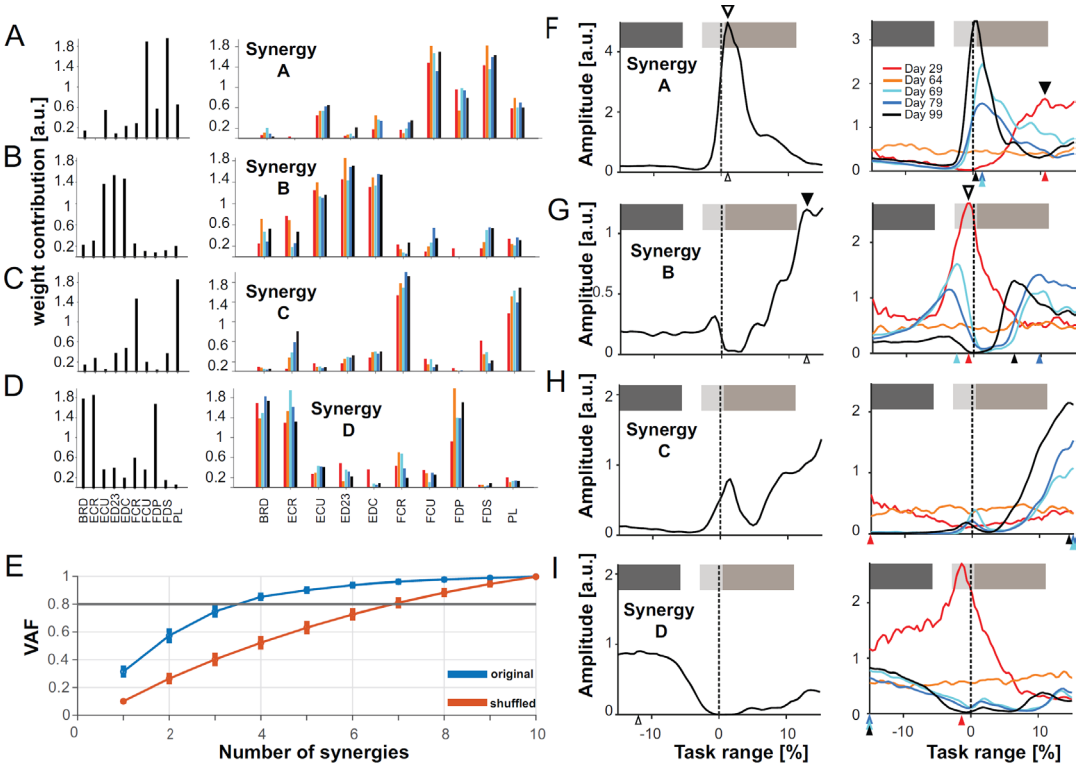

Fig. 6: Synergy weights & Temporal activation coefficients of monkey A.

(A-D) Synergy weights for each extracted muscle synergy. Plotted are the synergy weights for each muscle for one control day before (left column) and 5 landmark days after TT surgery (right column). (E) 'Variance Accounted For' (VAF) for the original and shuffled data. Four muscle synergies that accounted for more than 80% of the variance were extracted from the data. Black horizontal lines demarcate the 80% threshold. (F-I) Plotted are the time varying activation coefficients of the muscle synergies over task range [%] before (left column) and after TT (right column; shown are the activation coefficients for 5 landmark days). Horizontal gray bars mark the three behavioral periods (hook, grasp and release, respectively). Filled triangles in (F) and (G) indicate the maximum amplitude for synergy A (finger flexor synergy) just after TT (finger extension) and synergy B (finger extensor synergy) before TT (finger extension), while open triangles indicate the maximum amplitude for synergy A before (finger flexion) and synergy B just after TT (during flexion). Small triangles indicate the landmark days. Profiles are aligned on "object 1 hold off" at zero percent task range [%].

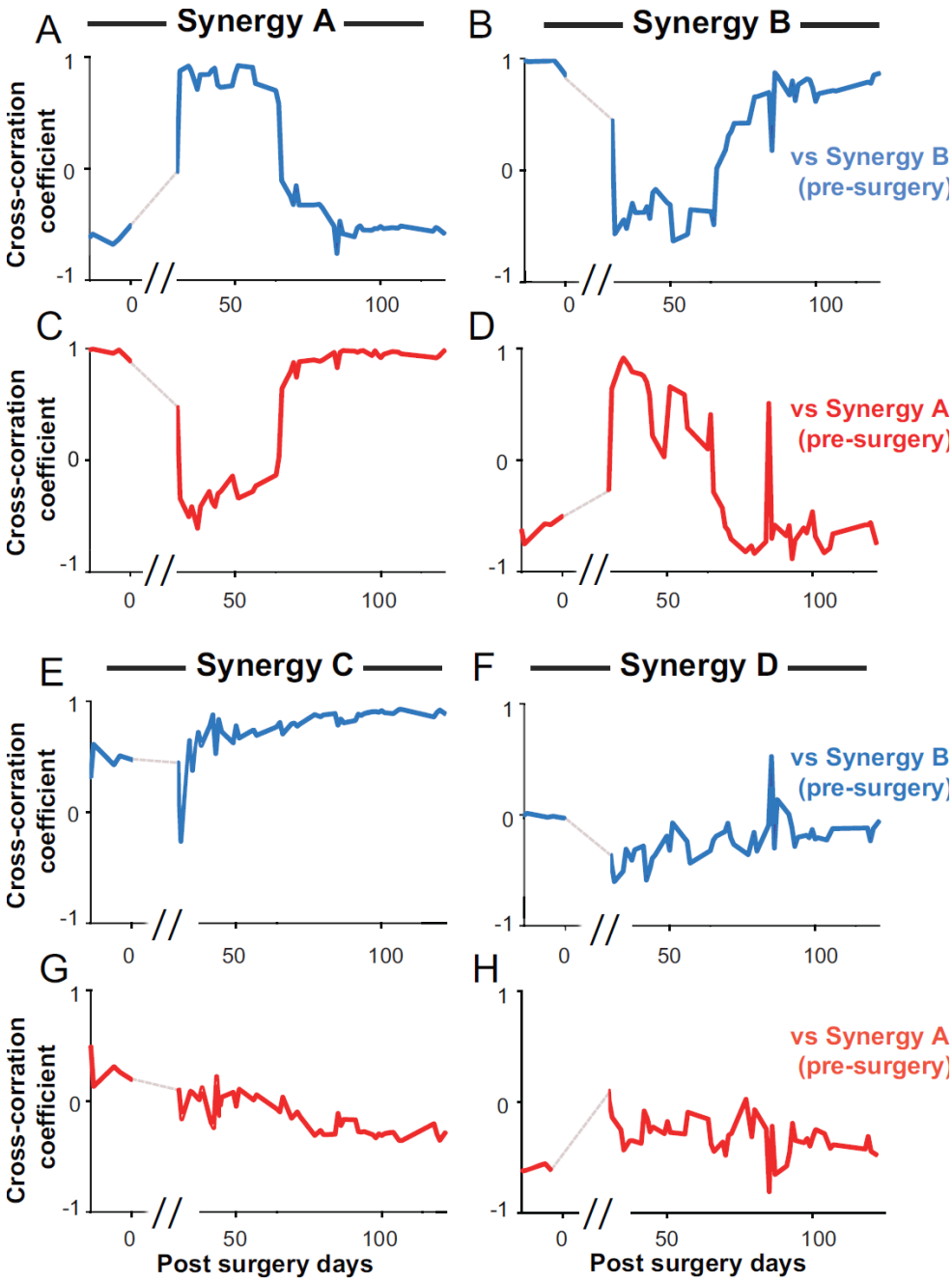

Fig. 7: Cross-correlation of muscle synergies.-
Cross-correlation coefficients were plotted over experimental days with respect to tendon surgery (Monkey A). The // represent the recovery period in which no recordings were taken. Synergies were cross-correlated with either synergy A (finger flexor synergy: C, D, G, H in red) or synergy B (finger extensor synergy, A, B, E, F in blue).

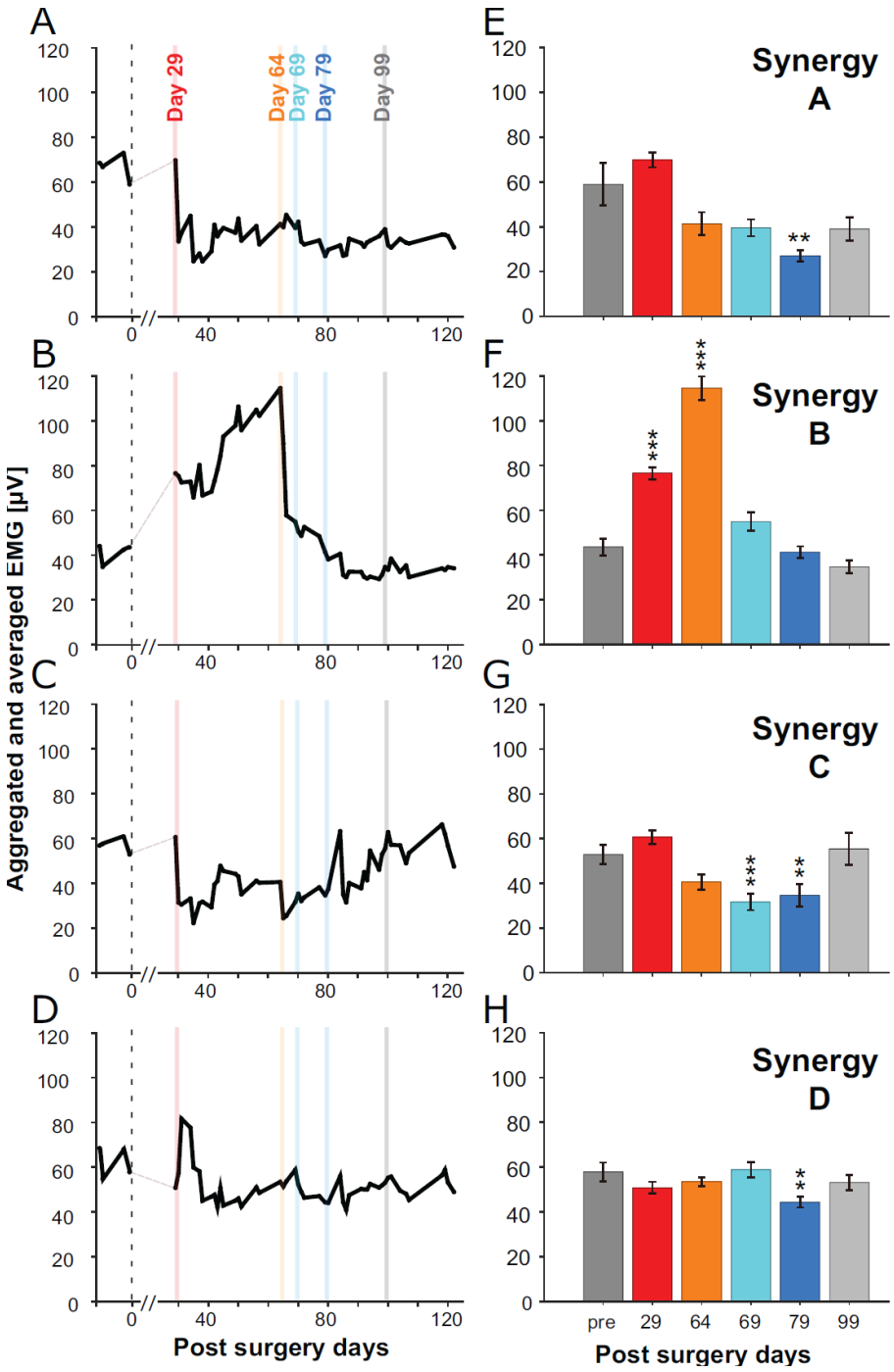

Fig. 8: Aggregated and averaged electromyography.

Aggregated and averaged electromyography (EMG) activities of the main muscles contributing to each of the four synergies for each recording day (Monkey A). EMG activity between -15% and +15% task range was summed for the contributing muscles and then averaged for each recording session. Left column: (A) synergy A, contributing muscles: flexor digitorum superficialis (FDS) and flexor carpi ulnaris (FCU); (B) synergy B, contributing muscles: extensor

digitorum communis (EDC), extensor digitorum-2,3 (ED23), and extensor carpi ulnaris (ECU); (C) synergy C, contributing muscles: palmaris longus (PL) and flexor carpi radialis (FCR); and (D) synergy D, contributing muscles: flexor digitorum profundus (FDP), brachioradialis (BRD), and extensor carpi radialis (ECR). Vertical bars represent landmark days (red numbers at the top show actual recording days with respect to tendon transfer surgery). Right column: mean and standard error of the mean for landmark days. *$p < 0.01$, **$p < 0.001$, ***$p < 0.0001$ after Bonferroni correction ($\alpha = 0.01$).

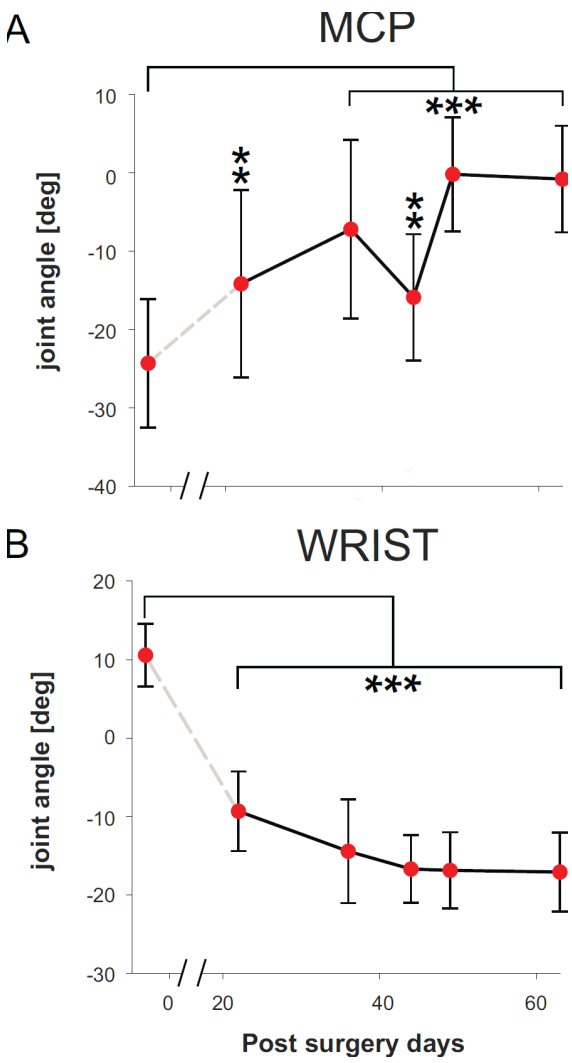

Fig. 9. ***Changes in Monkey B's Joint Angles Following Tendon Transfer (TT).***

Shown are the changes in the angle of two key joints in monkey B before and after TT surgery (mean of 20 trials ±SD for each landmark day, taken 83ms before food touch). The angle at the metacarpophalangeal (MCP) joint (A), responsible for finger extension, steadily increased following surgery (indicating increased finger extension). Concurrently, the wrist joint angle (B) decreased, indicating wrist flexion. Statistical analysis confirmed these changes were significant (ANOVA, $\alpha = 0.01$, $p < 0.0001$). This coordinated movement pattern suggests a potential compensatory strategy employed by the monkey to achieve finger extension during the grasping tasks. // represents the monkeys' recovery period in which no recordings were taken.

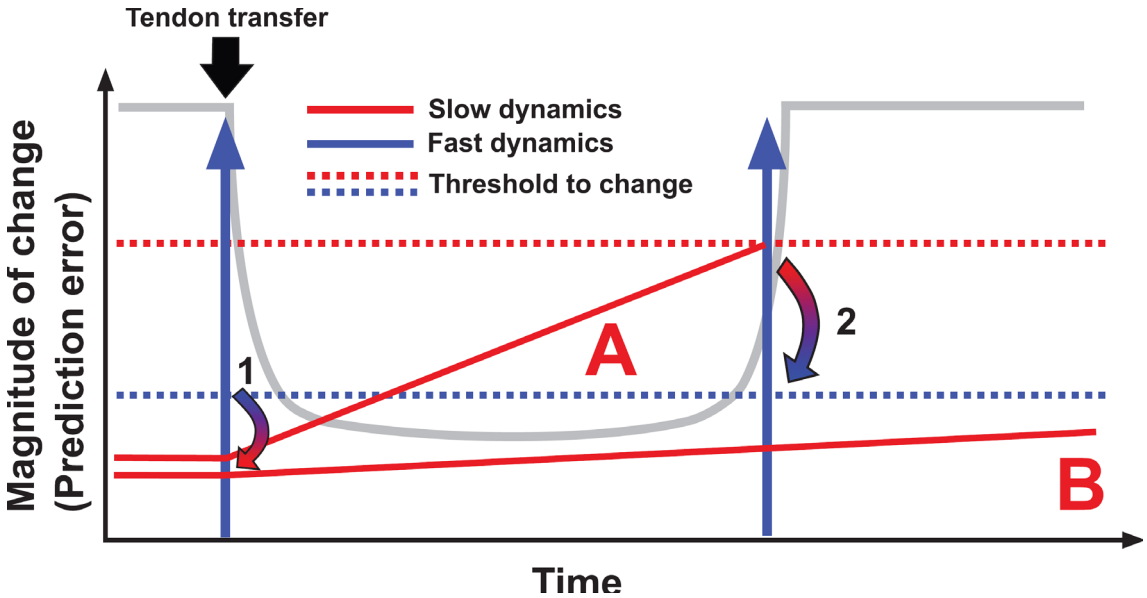

Fig. 10: Sensorimotor adaptation model following tendon transfer. Schematic depicting the hypothesized interaction between rapid and gradual adaptation processes in the central nervous system following a significant sensory prediction error (SPE) induced by tendon transfer (TT). Our model incorporates multiple TT adaptation processes with varying timescales, encompassing both fast and slow dynamics. Tendon transfer surgery (black arrow) necessitates adjustments in finger muscle coordination, particularly a shift in the timing of activity between flexor and extensor synergies (left blue arrow). These changes exceed a critical threshold (blue dotted line), triggering slow dynamic adaptations (A and B, blue and red arrow 1). Adaptation A is faster and aims to maintain the results of the initial fast adaptation (potentially maladaptive). Meanwhile, a slower process B (background) gradually builds a new behavioral component for “good enough” task performance. This new component only becomes apparent after a second fast adaptation (second blue arrow) is triggered by process A reaching another threshold (2). At this point, the cumulative costs of the maladaptive behavior become unacceptable. The gray line represents the observed changes of cross-correlation coefficients (electromyography and temporal activation coefficients of muscle synergies).